The Norian magmatic rocks of Jabuka, Brusnik and Vis Islands (Croatia) and their bearing on the evolution of Triassic magmatism in the Northern *Mediterranean*

M. Velicogna[a], A. De Min[b], M. K. Prašek[c], L. Ziberna[c], V. Brombin[d], F. Jourdan[e], P.R. Renne[f], D. Balen[g], M. Grégoire[h] and A. Marzoli[a]

[a]Department of Land, Environment, Agriculture and Forestry, University of Padova, Viale dell'Universita' 16, 35020 Legnaro, Italy; [b]Department of Mathematics and Geosciences, University of Trieste, Via Weiss 8, 34127 Trieste, Italy; [c]Department of Earth and Planetary Sciences (EPS), McGill University, 3450 University Street, H3A 0E8, Montreal, Québec, Canada; [d]Department of Physics and Earth Sciences, University of Ferrara, Via Saragat, 144122 Ferrara, Italy; [e]School of Earth and Planetary Sciences, Curtin University, 6845, Perth, Western Australia, Australia; [f]Department of Earth and Planetary Science, University of California, Berkeley, 307 McCone Hall, 94720-4767, Berkeley, CA, USA; [g]Department of Geology, Faculty of Science, Division for Mineralogy and Petrology, University of Zagreb, Horvatovac 95, HR-10000, Zagreb, Croatia; [h]Géosciences Environnement Toulouse, CNRS-CNES-IRD-Université Paul Sabatier, Observatoire Midi Pyrénées, 31400 Toulouse, France

ABSTRACT

The Norian magmatic rocks of Jabuka, Brusnik and Vis Islands (Croatia) and their bearing on the evolution of Triassic magmatism in the Northern Mediterranean. The magmatic rocks from Jabuka, Brusnik, Vis Islands and the submerged Brusnik plateau have been investigated to define their age and genetic affinity, identifying their role in the geodynamics of the Adria Plate. The plutonic and lava flow samples have been characterized for their petrography, mineral chemistry, whole rock major and trace elements, and Sr and Nd isotopic compositions. The two samples with the freshest plagioclase crystals have been selected for $^{40}Ar/^{39}Ar$ analysis, which gave ages of 221.5 ± 2.5 Ma (Brusnik) and 227 ± 5 Ma (Jabuka), similar to those of the Triassic magmatism from the northern part of the Adria Plate and neighbouring territories. Geochemical and isotopic data suggest that the magmatism dominantly sourced from spinel peridotites variously metasomatized during pre-Mesozoic subduction events. Furthermore, the investigated rocks evidence interactions of the magmas with Mid-Late Triassic evaporites. The comparison with other coeval magmatic occurrences from the Adria Plate and its edges shows that the subduction signature of the Triassic within-plate magmatism is mainly related to the evolution of the upper mantle of the Adria Plate.

ARTICLE HISTORY
Accepted 19 November 2022

KEYWORDS
Triassic magmatism; adria plate; geodynamic setting; basaltic andesite; brusnik; vis; jabuka

Introduction

Recent studies of the Mid-Late Triassic magmatism in the Adria Plate have been mostly focused on the magmatic bodies from northern Adria, now in the European Alps (e.g. Casetta et al. 2018a, 2018b; Lustrino et al. 2019; Storck et al. 2019; De Min et al. 2020). However, there is also growing evidence that the Mid-Late Triassic magmatism was quite widespread as it has been recognized for example in Calabria and Sardinia (southern Italy), the Northern Apennines (central Italy), and in the Dinarides (Croatia, Slovenia; Dobnikar et al. 2002; Beccaluva et al. 2005; Slovenec and Šegvić 2018, 2021). This magmatism was associated with an extensional phase within the Pangea supercontinent, which is considered to be a precursor of its break-up (e.g. De Min et al. 2020).

The Mid-Late Triassic Adria magmatism was probably formed during two main magmatic pulses, the first one during the Ladinian and the second one during the Norian. In the Alps, the first pulse (~238 Ma) is represented by intrusive rocks from Italy (Figure 1; Predazzo, Monzoni, and external Gabbro unit of Ivrea-Verbano complexes; e.g. Finero; Lu et al. 1997; Storck et al. 2019) and Austria (Figure 1; Karawanken; Miller et al. 2011), together with basaltic flows and dykes mainly cropping out in and close to the Dolomites (northern Italy, Southern Alps; Figure 1; e.g. Casetta et al. 2018a; Casetta et al. 2018b; De Min et al. 2020). The second pulse of Norian age (~220 Ma) is mainly represented by basalts of the Brescian Prealps (Southern Alps; Cassinis et al. 2008), by few lamprophyric dykes in the Dolomites (Figure 1; e.g. Casetta et al. 2018a, Casetta et al. 2018b, Casetta et al. 2019, Casetta et al. 2021; Storck et al. 2019; De Min et al. 2020), and by the Karawanken pluton (Figure 1; Visonà and Zanferrari 2000). From a geochemical point of view, the magmas show an apparent subduction affinity and have been considered by some authors as an expression of back-arc magmatism (e.g. Stampfli and Borel 2002; Csontos and Vörös 2004; Doglioni and Carminati 2008). However, other studies

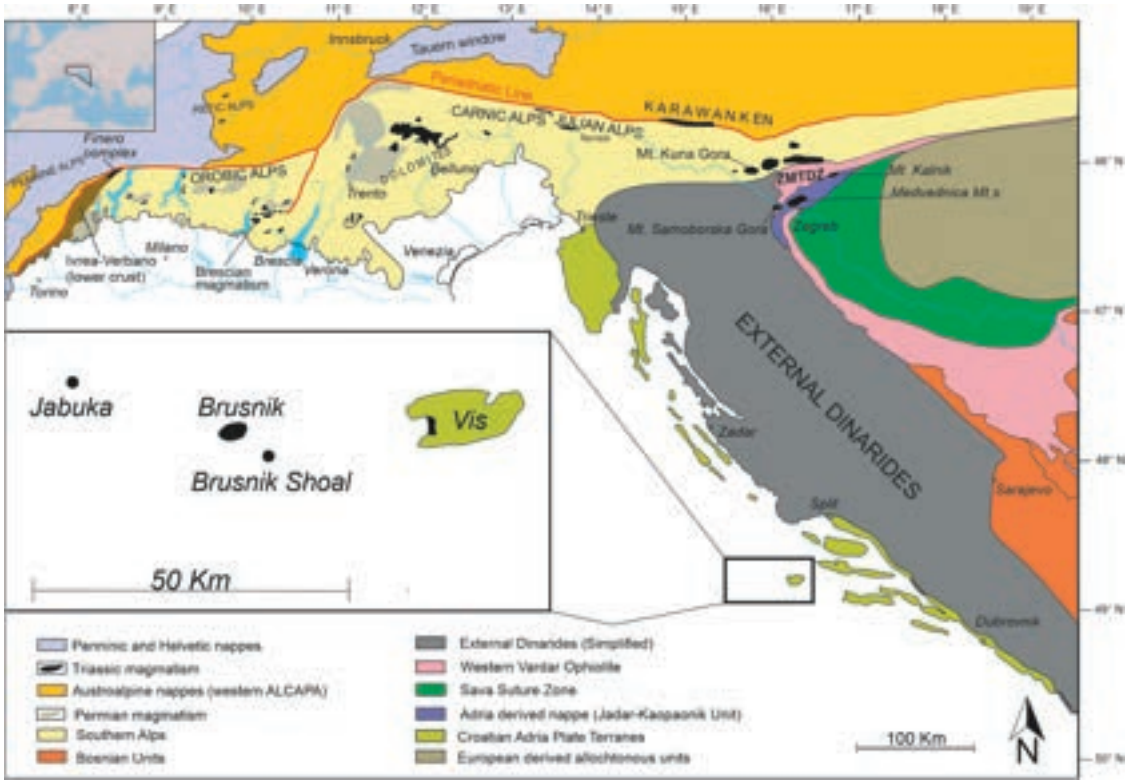

Figure 1. Geological sketch of the north-eastern part of the Adria Plate and nearby areas (modified after Juračić et al. 2004; Palinkaš et al. 2010; Slovenec and Šegvić 2018, 2021; De Min et al. 2020). The inset shows the area under investigation composed by the submerged plateau of Brusnik Shoal and by the islands of Jabuka, Brusnik and Vis. ZMTDZ is the Zagorje-Mid-Transdanubian Zone.

pointed out that this magmatic event was associated with transtensive to extensional tectonics and suggested that the subduction-related features are inherited from previous events, which modified the mantle sources (Beccaluva et al. 2005; Bonadiman et al. 1994; Casetta et al. 2018a, 2018b, 2021; Lustrino et al. 2019; De Min et al. 2020). In fact, the Mid-Late Triassic magmatism of the Adria Plate represents a good example of calcalkaline, high-K calcalkaline and potassic-ultrapotassic magmatic series recorded in extensional areas post-dating subduction processes (Lustrino et al. 2019).

This work focuses on a small group of Triassic magmatic bodies that crop out on islets (Jabuka, Brusnik and Vis Islands) and in a small underwater plateau (Brusnik Shoal) of the Adriatic Sea (Croatia; Figure 1), all located in the easternmost part of the Adria Plate (Adriatic Unit according to Slovenec et al. 2011; Slovenec and Šegvić 2021). These magmatic occurrences probably were part of a more widespread magmatic event that was buried during the Dinaric orogenesis, as testified by the large amount of gabbroic material underplated under the Adriatic Sea (Mancinelli et al. 2022). Given their relative distance from the Alpine counterparts, the magmatic rocks of these Croatian Islands could shed new light on the Triassic magmatism of the Adria plate, helping to better understand the Mesozoic geodynamics of the Mediterranean area before the break-up of Pangea. This study aims also to improve our understanding on the generation of extensional magmatism from subduction modified mantle sources.

In this work, we provide new petrographic observations, mineral chemistry, whole rock major and trace element and Sr-Nd isotope data, and $^{40}Ar/^{39}Ar$ ages for the intrusive, hypabyssal, and effusive magmatic rocks from the Adriatic Sea of Croatia. The aim is to characterize the Adriatic Magmatic Islands (hereafter AMI) from a petrological perspective to define their geodynamic affinities, source characteristics, possible contaminants and to use $^{40}Ar/^{39}Ar$ age data to determine the timeframe of the magmatism. Furthermore, the results will be compared to the Triassic magmatism of the northern Adria Plate to have a clearer perspective of how much and how extensively pre-Triassic subduction events modified the upper mantle that underlies the Adria Plate at the northern margin of Gondwana.

Geological background

In the Adriatic Sea, which represents a border of the European continental platform, magmatic outcrops are rare and are only found on the Croatian Islands of

Jabuka, Brusnik and Vis (Figure 1). Magmatic rocks on the studied islands are, from West to East, (1) intrusive bodies on Jabuka, (2) shallow hypabyssal intrusions partially cut by leucocratic dikes and by gabbroic breccias on Brusnik, and (3) variably altered effusive rocks on Vis. The presence of a magmatic shoal composed of basalts, andesites and basaltic trachy-andesites between Jabuka and Brusnik seems to strengthen the view of a common and connected origin of the magmatic products from the three islands (Juračić et al. 2004).

Several authors (e.g. Grandić et al. 2004, 2013; Brkić et al. 2011; Kulušić and Borojević Šostaric 2014; Pikelj et al. 2015) suggest that the magmatic bodies and underlying salt diapirs have been exhumed and partially tilted during the last phases of the Cenozoic Dinaric orogeny, during which compressional forces reactivated the Mesozoic extensional faults causing uplift of saline diapirs. During exhumation, the magmatic bodies pierced Jurassic, Cretaceous, Palaeogene, and Neogene sedimentary rocks. One of the saline diapirs partially crops out in Vis and is composed of evaporites of Ladinian-Norian age as evidenced by palynological data and structural studies (Koch and Belak 2003). The oldest unit of the evaporites contains basaltic tuffs, suggesting that the magmatism was contemporaneous with the Mid-Late Triassic evaporites. A second salt diapir discovered with geophysical surveys lies under Jabuka Island (Pikelj et al. 2015).

The Adriatic Magmatic Islands of Jabuka, Brusnik and Vis are located in the middle of the Adriatic Carbonate Platform and are part of the Adria Plate. Adria presently comprises the southern and eastern Alps, the Adriatic and Ionio Units (north-eastern to south-eastern Italy), Istria peninsula (Croatia and Slovenia), and several islands and parts of the coast of south-western Croatia (Schettino and Turco 2011). Although it is widely assumed that Adria originally derived from the northern edge of the Gondwana plate, its Mesozoic and Cenozoic geodynamic evolution is still debated (De Min et al. 2020, and references therein). Several authors suggest that during the Permian, the northward subduction of the Palaeotethys under the southern part of Laurussia formed a mechanism that detached a ribbon-like terrane from northern Gondwana, resulting in the opening of the Neothetys (e.g. Golonka 2004; Stampfli and Kozur 2006). The subduction rollback created several oceanic ridges, generally NW-SE elongated, i.e. Meliata, Maliac, Pindos (Stampfli and Borel 2002) or Vardar and Pindos (Csontos and Vörös 2004). In particular, the Meliata rift may have affected the continental plate from the Balkans to the Ivrea-Verbano zone, Southern Alps, where Permian basic magmatism is widespread (e.g. Peressini et al. 2007; Boscaini et al. 2020). Recently, Mancinelli et al. (2022) suggested a back-arc genesis for the AMI magmatism, assuming a Permian age of the basalts. Bianchini et al. (2018) also suggested a subduction origin for the Permo-Triassic magmatism of the Southern Alps, which occurred after the final stages of westward subduction and possibly related to extreme slab verticalization and/or with slab break off.

On the contrary, Bortolotti and Principi (2005), Schmid et al. (2008), Muttoni et al. (2009) and Maffione and van Hinsbergen (2018) suggested that the Neotethys was formed only by one branch. The former authors use the term 'Eastern Tethys' or 'Neotethys' to describe all the oceanic realms located in an area south-east of the Alpine Tethys and the future Western Alps that opened during and after the Permian to Triassic closure of the Paleotethys. The reconstruction of Schettino and Turco (2011) suggests that the spreading centre of the Neotethys was linked to the extensional system of Central Pangea by a triple junction, similar to the triple point suggested by Muttoni et al. (2009) that connected the Neothethys, Paleotethys and the Intra-Pangea Dextral Shear.

Triassic magmatism in the adria plate and nearby areas

The igneous rocks of AMI are part of a large Permo-Triassic magmatic rifting system, which produced gabbro-diorite-syenite-granite formations in the Dinarides and basalt-andesite-dacite formations within the Adriatic carbonate platform (Pamić et al. 2002), which is of Permian to Eocene age (Vlahović et al. 2005). Pamić et al. (2002) suggested that these Permo-Triassic magmatic occurrences could be related to the initial rifting phases associated with the incipient instability of Pangea. The magmatic bodies show large variability in composition and morphological features. Pamić (1984) divided them into seven main sub-provinces with different petrologic affinities and one that includes independent small volcanic occurrences. However, he defined the magmatic groups without considering the Triassic geodynamic and geologic setting. In fact, most of the sub-provinces defined by Pamić (1984) are located in the Internal Dinarides and therefore are part of the Tisia Plate or occupy an extensional area between the Tisia and Adria plates, the Zagorje-Mid-Transdanubian Zone (ZMTDZ). The ZMTDZ represents a triple junction zone between the South-eastern Alps, the Tisia continental block and the Internal Dinarides (Figure 1). In the External Dinarides, only a few magmatic occurrences have been described (Juračić et al. 2004; Palinkaš et al. 2010). The magmatism of the Adriatic islands occurs in the first magmatic sub-province of Pamić (1984). Since

the focus of this work is on the magmatism outcropping in the Adria Plate and its margins, here we consider only these magmatic products and those of the ZMTDZ.

The magmatism of Jabuka, Brusnik and Vis has been previously dated using K/Ar (Balogh et al. 1994) and $^{40}Ar/^{39}Ar$ techniques (unpublished data referred to in De Min et al. 2009, and in Palinkaš et al. 2010). Balogh et al. (1994) focused on Brusnik and obtained an average K/Ar age of 205.4 ± 6.9 Ma, which has been roughly interpreted as the latest stage of crystallization after the intrusion. De Min et al. (2009) report Ar/Ar ages in a conference abstract but did not publish or discuss in detail the radio-isotopic age data. Palinkaš et al. (2010) refer in a field-guide to biotite and K-feldspars $^{40}Ar/^{39}Ar$ ages for Jabuka and Brusnik, and Vis, which range from 276 ± 1.7 Ma to 254 ± 2 Ma with one much younger age at 214 ± 0.9 Ma. However, data for these $^{40}Ar/^{39}Ar$ ages have never been published, hindering a detailed evaluation of their significance, particularly in the context that most rocks show some level of alteration which can significantly perturb the $^{40}Ar/^{39}Ar$ results (Verati and Jourdan 2014; Jiang et al. 2021).

Sampling

Thirty samples of plutonic rocks and lava flows have been collected in the islands of Jabuka, Brusnik, Brusnik shoal and Vis (Figure 2). Where possible, the samples have been hammered from the magmatic outcrops, while few others have been collected as rock fragments or big cobbles from the sea bottom or the shore, as close as possible to the outcrops.

The Jabuka Island is a small magmatic outcrop (Figure 2a), which probably represents the subaerial part of a mostly submarine magmatic edifice. The island is located 50 km north-west of Komiža (Vis Island). Jabuka shows vertical flanks and a complex system of jointing and cracks that impart a pseudostratified appearance (Golub and Vragovič 1975). The samples have been collected in the southern part of the island

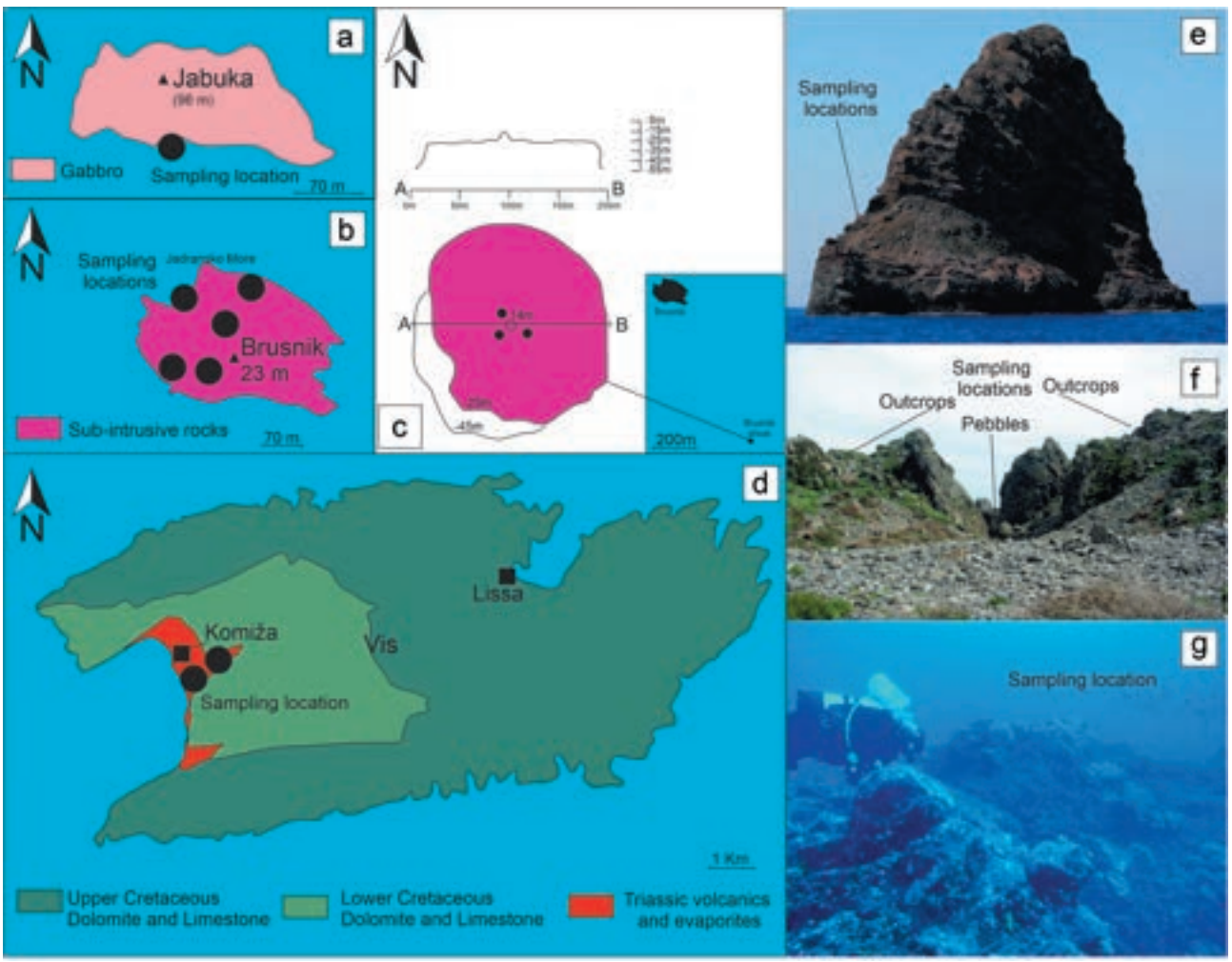

Figure 2. Sampling locations (black circles) in Jabuka (a, e), Brusnik (b, f), Brusnik Shoal (c, g) and Vis (d).

(42°59′48″ N and 15°17′24″ E; the only place that was safely reachable) from outcropping rocks and as loose material from the sea bottom at about 10 m below sea level. The outcrop was formed by gabbro that showed homogeneous texture and paragenesis. In some shallow areas, round conglomerates can be seen, appearing very similar to those found on Brusnik.

Brusnik (43°00′21″N, 15°48′04″ E) is located 24-km east of Vis (Figure 2b). The island is composed by dolerites and few felsic dykes (Garašić et al. 2001) with the presence of rare breccias of mafic magmatic rocks cemented by non-fossiliferous carbonates. The samples have been mainly collected from three places in the north-western part of the island. Two are proper outcrops of gabbroic rocks with homogeneous texture and large pyroxene and plagioclase crystals. Three pebbles (~20 cm) formed by gabbro similar to that of the outcrops have been collected on the north-western beach.

Brusnik shoal (42°59′37″N, 15°48′36″E; Figure 2c) is located 1.6 km south-east of Brusnik. The Brusnik shoal is a sub-circular platform with a diameter of about 200 m. Three samples have been collected from the top of the plateau at about 15 m below sea level during a diving session.

Among the AMI, Vis (Komiža = 43°02′33″N, 16° 05′24″E) is the biggest island and it is the closest to the mainland (Figure 2d). The main outcrop areas are small and located in the western part of the island near Komiža village and are represented by aphyric, slightly plagioclase-phyric or by highly altered and vescicular lava flows with vesicles filled by prehnite. The plagioclase-phyric flow outcrops close to the seashore, while the prehnite-rich flow can be found at higher altitude. Due to the small size of the outcrops, it is not possible to understand if they are part of the same lava flow field. Similar volcanic rock types can also be found as clasts in a small volcano-sedimentary sequence on the island.

Methods

Rock powders obtained at the Department of Mathematics and Geoscience of the University of Trieste (Italy) using an Iron Tungsten-alloy mortar, have been analysed at Mining Laboratory Services of the Bureau Veritas infrastructure (Vancouver, Canada). The same rock powders preparation procedure was applied at Department of Geology, Faculty of Science, University of Zagreb for an additional set of AMI samples. Before whole-rock analysis, the powders (0.2 g) were melted with lithium metaborate ($LiBO_2$)/tetraborate ($Li_2B_4O_7$) and dissolved in dilute nitric acid (HNO_3). The loss on ignition (LOI) in all samples was determined by the difference in weight after annealing at 1000°C for 4 h (Bureau Veritas procedures 4A, www.bureauveritas.com). Major elements were determined by inductively coupled plasma with emission spectroscopy (ICP-ES), while the trace elements were determined by inductively coupled plasma mass spectroscopy (ICP-MS). One part (0.5 g) of the sample was separated, dissolved in aqua regia (at 95°C), and analysed by ICP-MS for precious and base metals. Internal standards (natural rocks of known composition and natural pure quartz) were used to correct for matrix effect. Analytical precision was controlled using geological standard materials. Reference materials were certified by ACMELab laboratory, with a comparative analysis at CANMET (Canada Centre for Mineral and Energy Technology) with certified reference materials. Upper and lower limits of detection for each element analysed are readily available on the ACMELab Bureau Veritas commercial website. Blank measurements for all analyses were below the detection limits. Measured standard values and detection limits are summarized in Supp. Table A1.

Mineral analyses of selected samples were carried out using a Cameca-SX50 electron microprobe operating at 15 kV and 15 nA at the IGG–CNR, Padova (Italy). Counting times were 10 s for peak and 10 s for background and the spot size was ca. 2 μm. Natural and synthetic minerals were used as standards. The PAP Cameca program has been used to convert X-ray counts into weight percentages of the corresponding oxides. The results are considered accurate to within 2–3% for major elements and 9% for minor elements. The Fe^{2+} and Fe^{3+} contents in pyroxenes and amphiboles have been calculated according to Papike (1974).

Additional mineral analyses were obtained with a CAMECA SX100 EMP at the State Geological Institute of Dionýz Štúr in Bratislava (Slovakia). The operating conditions for EMP analysis were 15 kV accelerating voltage, 20 nA beam current and beam diameters typically between 3 and 5 μm. Standards included minerals, metals, and chemical compounds (wollastonite, TiO_2, Al_2O_3, Cr, fayalite, rhodonite, forsterite, LiF, Ni, V, willemite, NaCl, $SrTiO_3$, barite, orthoclase and albite). Detection limits for major elements are 0.01–0.02 wt.%. The matrix effects were corrected by the conventional ZAF (atomic number-absorption-fluorescence) method.

Samples for $^{40}Ar/^{39}Ar$ analyses were crushed, sieved and cleaned with ethanol and deionized water. Plagioclase crystals were further separated using a Frantz magnetic separator and carefully picked under the binocular microscope. Samples and Fish Canyon sanidine standards were irradiated in the Cd-shielded (to minimize undesirable nuclear interference reactions) CLICIT facility of the TRIGA reactor at Oregon State University, USA. $^{40}Ar/^{39}Ar$ analyses were performed at

the Berkeley Geochronology Center with a MAP215 spectrometer. Step heating was achieved using a CO_2 laser. The gas was purified in a stainless-steel extraction line using two C-50 getters and a cryogenic condensation trap. Ar isotopes were measured in static mode using an analog Balzers electron multiplier mostly using 10 cycles of peak-hopping. Ar isotopic data corrected for blank, mass discrimination and radioactive decay are given in the supplementary material. Individual uncertainties in Supp. Table A2 are given at the 1σ level, while mini-plateau ages (Supp. Table A2) are given at the 2σ level and are calculated using the mean of all the plateau steps, each weighted by the inverse variance of their individual analytical uncertainty. Inverse isochrons include the maximum number of consecutive steps with a probability of fit ≥ 0.05. The uncertainties on the $^{40}Ar^*/^{39}Ar$ ratios of the monitors are included in the calculation of the integrated and plateau age uncertainties, but not those related to the age of the monitor and to the decay constant (internal errors only, see discussion in Min et al. 2000). Full uncertainties including all sources of systematic are also provided and indicated in brackets as ± [1.5] Ma. All ages and error propagation have been recalculated according to Renne et al. (2010), (2011). Detailed $^{40}Ar/^{39}Ar$ results are shown in the supplementary material and summarized in Supp. Table A2.

Nd-Sr isotopic data were obtained at Géosciences Environnement Toulouse Observatoire Midi-Pyrénées (GET-OMP) at the Université Toulouse III (Toulouse, France). Approximately 100 mg of powder was weighed in a teflon beaker and dissolved in a mixture $HF/HClO_4$ 1:1 following the Yokoyama et al. (1999) dissolution protocol. REE and Sr were extracted from the matrix using a combination of Sr-Spec and Thru-spec resins. An equivalent of 500 ng Sr and 300 ng REE mixtures were run on a TRITON Plus Thermo-Scientific spectrometer following protocols of Li et al. (2011, 2012): first Sr then Nd corrected from Sm interferences. Doped SRM987 (Rb) and La Jolla (Sm) isotopic standards were regularly run in the TIMS lab and give reproducibility of about 0.51848 ± 8 (n = 20) for La Jolla and 0.710278 ± 16 (n = 46) for SRM987. JNdi Nd standard have also been run during the measurements and give respectively 0.512105 and 0.512111. Typical blanks are 50 pg for Nd and 150 pg for Sr. BCR2 Geostandard has been processed the same way as the analysed samples (dissolution-purification-loading-measurements).

Petrography

The intrusive samples from Jabuka are holocrystalline and show a medium-coarse grain size with subipidiomorphic texture (Figure 3a). The rocks are quite altered and appear to be slightly hydrothermalized. Plagioclase is often zoned and seriticitized, however large portions of the crystals are unaltered. The pyroxenes are mainly augite and rarely pigeonite and are slightly altered to uralite, amphibole or chlorite. Rare opaque minerals (magnetite) are present as small crystals. Finally, rare feldspar-quartz intergrowths could be found. Apatite has been found as little needles included in plagioclase.

The hypabyssal rocks from Brusnik appear less altered than those from Jabuka (Figure 3b). They are holocrystalline and show an intergranular texture. Plagioclase is often idiomorphic, slightly zoned and partly altered into sericitic products. Clinopyroxene and pigeonite are both present as idiomorphic and 'spinifex'- like crystals. Opaque minerals are scarce and are recognized as magnetite. Rare alkaline feldspar and quartz appear confined to the groundmass. Vesicles and/or small veins filled by secondary zeolites and prehnites are rare.

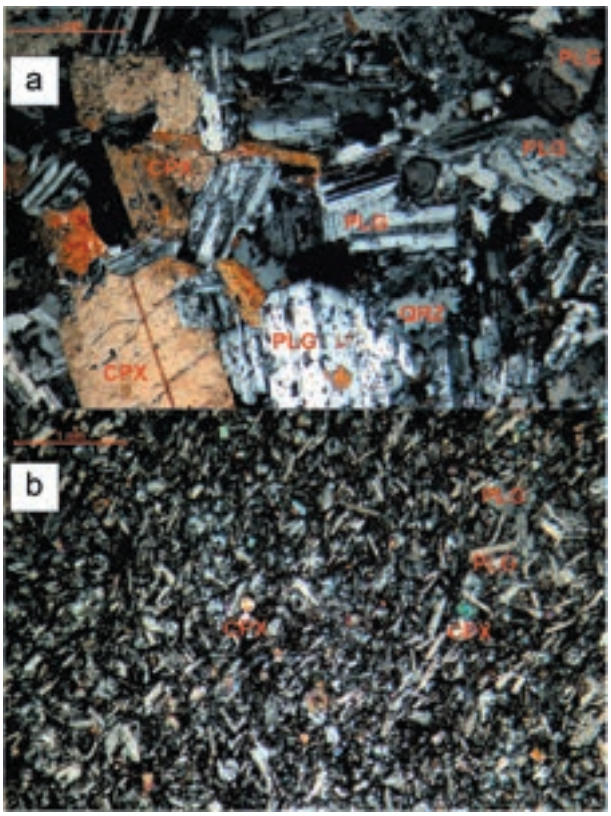

Figure 3. Representative crossed polars transmitted light microphotographs of AMI samples. (a) an intrusive Brusnik sample (BK4A) that shows the generally unaltered and idiomorphic plagioclase crystals with polysynthetic germination and concentric zonation; poorly altered pyroxene and small quartz intergrowths; (b) an aphyric Vis sample (VK16a) with little-altered clinopyroxene and plagioclase crystals.

The Brusnik Shoal samples show similar mineral paragenesis to those from Brusnik and Jabuka but with a generally finer-grained texture and a higher grade of alteration (Figure 3c). Plagioclase is the largest and most abundant phase and shows a high degree of alteration in sericitic products. Chlorite is the second most abundant mineral and is often associated with biotite as alteration products of pyroxenes and amphiboles. Opaques recognized as magnetite and ilmenite are present as primary and secondary minerals.

The volcanic rocks from Vis are represented by aphyric, slightly plagioclase-phyric samples or by highly altered lava flows with vesicles filled by prehnite (Figure 3d). In the plagioclase-phyric samples the main mineral is plagioclase that occurs as sericitized macrocrystals and fresh microcrystals. Clinopyroxene is relatively abundant and is generally unaltered, idiomorphic, and optically unzoned. Chlorite and opaques are present but not abundant. The aphyric samples are composed by plagioclase and pyroxene microcrystals that are quite altered, being replaced by sericitic and chloritic products, respectively. Secondary calcite is also present as alteration phase of clinopyroxene.

Mineral chemistry

Pyroxene

Pyroxenes have been analysed in samples from Jabuka and from Brusnik (Supp. Table A3). Following the classification of Morimoto (1988), most analysed pyroxenes are augites (Figure 4a). However, among the Jabuka samples, there are two pigeonites and one hedenbergite, consistent with microscope observation, while in the Brusnik samples, two ferraugites and one diopside have been analysed (Figure 4a). The augites show Mg# between 0.43 and 0.60, the ferroaugites between 0.32 and 0.36, while the Mg# of the analysed diopside (Brusnik), hedenbergite (Jabuka) and pigeonites (Jabuka) are 0.63, 0.27 and 0.50, respectively [Mg# = Mg/(Mg + Fe^{2+}), where the Fe^{2+} has been recalculated after (Papike 1974)]. All the crystals are characterized by low TiO_2 (0.10–0.60 wt.%). Pyroxenes plots close the Skaergaard intrusion line (Coleman 1978) that is typical of tholeiitic series, with the exception of the Ca-rich crystals (i.e. hedenbergite, diopside and high Ca-augites). Furthermore, the hedenbergite shows high Na_2O (1.3 wt.%).

Plagioclase and K-feldspars

The analysed plagioclase ranges from An_{84-63} (early crystallization; phenocryst cores; An = mol% anorthite; Supp. Table A3; Figure 4b) to An_{60-40} (late crystallization; phenocryst rims and microcysts; Supp. Table A3; Figure 4b). In particular, the most An-rich compositions are shown by samples from Brusnik (An_{84-76} and An_{54}; early and late crystallization), where albitized (and probably spilitized) plagioclase (An_{29-8}) and microlites of K-feldspar (Or_{97}) have also been found. The less altered sample from Jabuka shows plagioclase in the range An_{63-47}, which is slightly less calcic than plagioclase compositions of An_{75-57} reported in Balogh et al. (1994) for the same rocks. Finally, the microphenocrysts analysed from a Vis sample yield An_{58-49}.

Amphiboles

Three secondary amphiboles from Jabuka have been selected and analysed (Supp. table A3). Following the classification of Hawthorne et al. (2012), they are part of

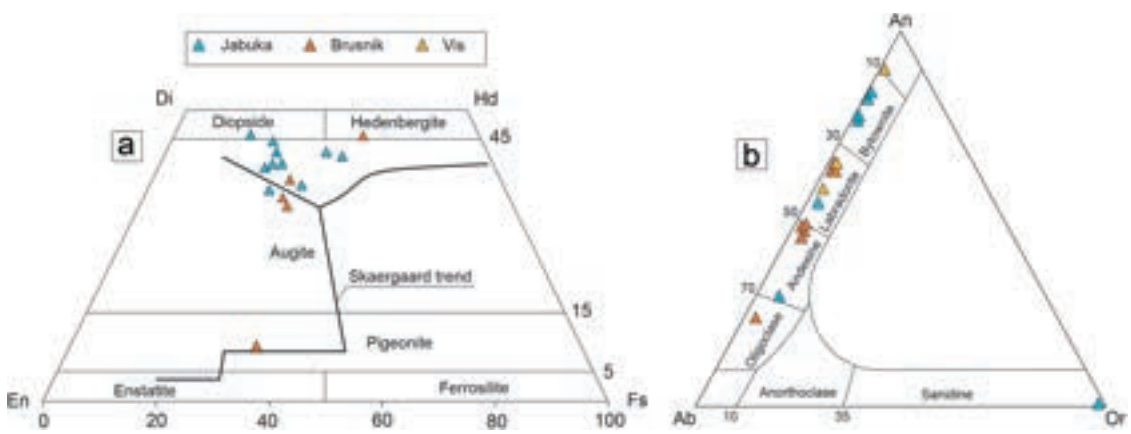

Figure 4. a) Morimoto (1988) classification for pyroxenes from Jabuka (J3); light blue triangles), Brusnik islands (BK4A and BK8A; orange triangles). The continuous bold lines correspond to the Skaergaard trend (Coleman1978). b) Triangular plot for plagioclase feldspar classification of Jabuka (J3), Brusnik (BK4A and BK8A) and Vis (VK16a, yellow triangles).

the calcic group and fall in the ferro edenite, ferro-ferri hornblende and ferro-hornblende field. The ferro-edenite shows the highest TiO_2 and MgO (1.30 wt.% and 9.80 wt.%, respectively) and lowest MnO, FeO and CaO contents (0.36 wt.%, 21.99 wt.%, and 10.27 wt.%, respectively). Ferro-ferri hornblende and ferro-hornblende show similar FeO (25.17–26.68 wt.%), TiO_2 (0.28–0.44 wt.%) and CaO (11.58–11.61 wt.%), while they mainly differ in Al_2O_3 (4.56–7.85 wt.%) and MgO (6.88–4.12 wt.%) values. They show a high Al_2O_3/TiO_2 ratio that is typical of amphibole from calcalkaline magmas.

Oxides

In Brusnik (BK4A) one couple of ilmenite and magnetite crystals has been analysed (Supp. Table A3). The ilmenite shows FeO and TiO_2 contents of 47.5 and 50.69 wt.%, respectively, while the magnetite shows FeO and TiO_2 values of 85.1 and 6.51 wt.%, respectively. Only in this sample, it has been possible to calculate the oxygen fugacity (after Frost 1991), which resulted close to the QFM buffer (at −1.86 log units below the NNO buffer). Furthermore, three ilmenite (FeO ca. 48 wt.% and TiO_2 ca. 49 – wt.%) and three magnetite crystals (FeO ca. 88 wt.% and TiO_2 ca, 4 wt.%) from Jabuka samples have been analysed.

$^{40}Ar/^{39}Ar$ ages

The samples with the freshest plagioclase crystals (BKA and BR3 from Jabuka and Brusnik, respectively) were selected for $^{40}Ar/^{39}Ar$ analyses. The feldspars of samples BR3 (Brusnik) yielded a mini-plateau age of 219.5 ± 2.5 Ma (P-value = 0.69) including 55% of the total ^{39}Ar released (Figure 5a). However, we note that the age spectrum shows a pronounced tilde-shape pattern. Through experimental and numerical approaches, Verati and Jourdan (2014) and Jiang et al. (2021) showed that such a pattern represents the signature of sericite, where the latter tends to affect all the heating steps and lower the apparent age of a sample. Therefore, despite providing a 55% mini-plateau, this age is most likely a minimum age.

A second sample (BKA; Jabuka) provided a flatter overall age spectrum compared to BR3 and yielded a 55% mini-plateau age of 227 ± 5 Ma (P = 0.21) without showing an obvious tilde-shape sericite signature. Therefore, the apparent age of BKA plagioclase is considered slightly more reliable despite its low precision (Figure 5b).

Furthermore, low $^{37}Ar/^{39}Ar$ (0.5–9) for the mini-plateau steps of BR3 suggest that these are defined by a low-Ca feldspar, while plateau steps of BKA yielded higher $^{37}Ar/^{39}Ar$ (22–40), more consistent with the plagioclase compositions obtained by electron microprobe analyses. The mini-plateau ages are indistinguishable from the respective $^{39}Ar/^{40}$ vs $^{36}Ar/^{40}Ar$ isochron ages (228 ± 3 Ma and 220 ± 3 Ma for BKA and BR3, respectively), which yield initial $^{40}Ar/^{36}Ar$ values close to that of air (283 ± 5 and 288 ± 19, respectively).

In summary, none of the apparent ages are very robust, as would be the case for a plateau age (defined by >70% of released ^{39}Ar). Nevertheless, we conclude that these samples are likely contemporaneous but that the age of the magmatism is best approximated by the age of 227 ± 5 Ma obtained on sample BKA.

Whole-rock geochemistry

Classification

The intrusive Jabuka samples have been classified as gabbros based on their modal mineral composition. Even if coarse-grained Jabuka rocks may occasionally reflect some cumulate effect, like high Al_2O_3 in very

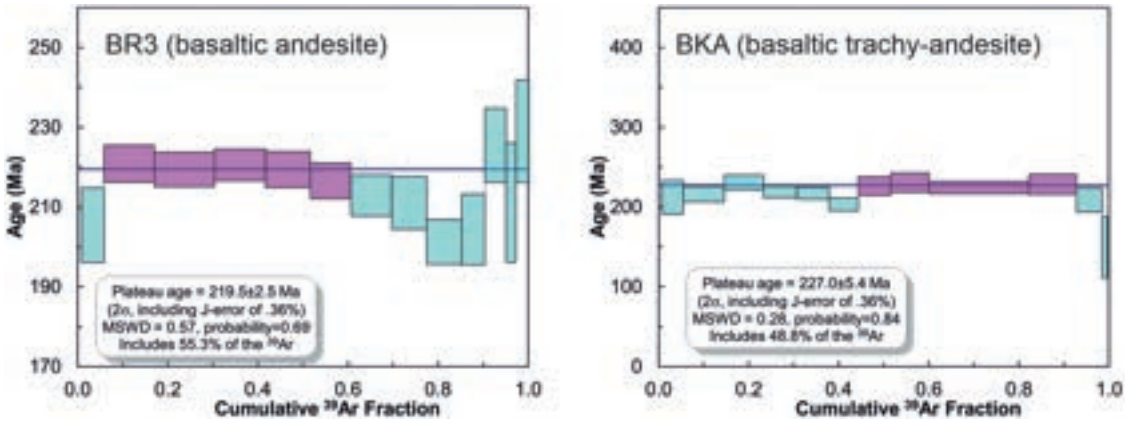

Figure 5. Apparent age spectra of plagioclase separate for BKA and BR3. Age in million years, Ma. Plateau steps are magenta, rejected steps are cyan and box heights are 2σ uncertainties.

feldspar-rich samples, their whole-rock major and trace elements composition are generally similar to the finer grained Brusnik and Brusnik shoal samples and to Vis volcanics (whole rock compositions are reported in Supp.Table A2). Therefore, all the samples including those from Jabuka are plotted and classified in the Total Alkali Silica (TAS; Figure 6a) classification diagram of Le Bas et al. (1992).

The samples show a spread in alkali content (Na_2O+K_2O = 3.87–8.96 wt.%) at similar SiO_2 (48.58–58.81 wt.%; Figure 6a). The selected samples mainly classify as basaltic andesite and basaltic trachy-andesite, two Vis samples fall in the trachy-basalt field (VK17 and VK20) and one in the basalt field (J5) (Figure 6a). A similar spread to the TAS diagram is also shown by the SiO_2 vs K_2O diagram (Figure 6b). More precisely, the majority of the Brusnik samples fall in the calc-alkaline field, a subgroup plots close to the boundary with the tholeiitic series and a second one straddles the boundary between the calc-alkaline and the high-K calc-alkaline fields. The Brusnik shoal and Jabuka samples show high K_2O contents plotting in the calc-alkaline and high-K calc-alkaline series fields. This is in contrast with the mineralogy of the Jabuka samples, where the presence of pigeonites indicates a tholeiitic affinity. Finally, Vis samples (except one) fall in the high-K calc-alkaline and in the shoshonite fields. Considering the Peacock index (also known as Alkali-Lime Index; Peacock 1931; Arculus 2003) based on the combined Total Alkali (Na_2O+K_2O) and CaO versus silica diagrams (not shown), the samples fall in the alkali-calcic and calk-alkaline fields as the Triassic basalts from the Southern Alps (Dolomites).

Major elements

The AMI samples appear quite evolved, showing Mg# values [Mg# = Mg/(Mg + Fe^{2+}) calculated assuming a Fe_2O_3/FeO ratio of 0.21 following (Cottrell and Kelley 2011)] that span from 0.25 to 0.37 (Supp. Table A1). Generally, the major element vs Mg# diagrams show no clear correlations. Particularly scattered are Mg# vs CaO (Supp. Figure 1b) and Na_2O (Supp. Figure 1c), which could be related to secondary effects (see later in 'Crustal, Magma-seawater or evaporite contaminations?' chapter).

Trace elements

The chondrite-normalized (CN; Boynton 1984) REEs patterns are shown in Figure 7. The samples are slightly enriched in light REEs (LREE), while the medium and heavy REE (MREE and HREE, respectively) show nearly flat patterns. In particular, the Jabuka, Brusnik and Brusnik Shoal samples show similar La/Sm_{CN} ($La/Sm_{CN(Jabuka)}$ = 2.15–2.80, $La/Sm_{CN(Brusnik)}$ = 1.91–2.84 and $La/Sm_{CN(Brusnik\ Shoal)}$ = 2.11–2.40), while Vis volcanic rocks show slightly higher values ($La/Sm_{CN(Vis)}$ = 2.59–3.42). On the contrary, the MREE and HREE ratios are similar for all samples (Sm/Dy_{CN} = 1.40–1.93; Dy/Yb_{CN} = 1.00–1.27; average values). The La/Yb_{CN} ratio varies from ca. 3.8 (Jabuka) to 4.2 (Brusnik and Brusnik Shoal) and 4.9 (Vis). The majority of the samples show a similar negative Eu anomaly (Eu/Eu* = 0.90–0.68; Eu* = (Sm_{CN} + Gd_{CN})/2), which may result from plagioclase fractionation.

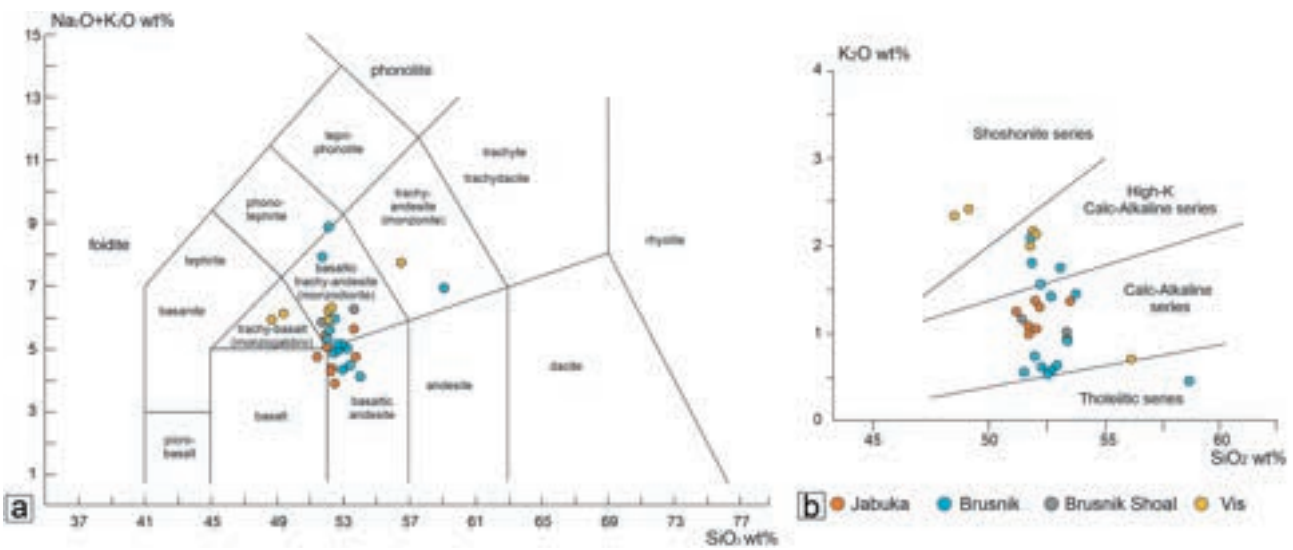

Figure 6. a)Tas (Total Alkali Silica) diagram after Le Bas et al. (1992) for the analysed samples. b) K_2O vs. SiO_2 wt.% classification (Peccerillo and Taylor 1976; modified). Orange circles = Jabuka; light blue circles = Brusnik; grey circles = Brusnik Shoal; yellow circles = Vis. The whole-rock compositions are normalized to 100 wt.% anhydrous.

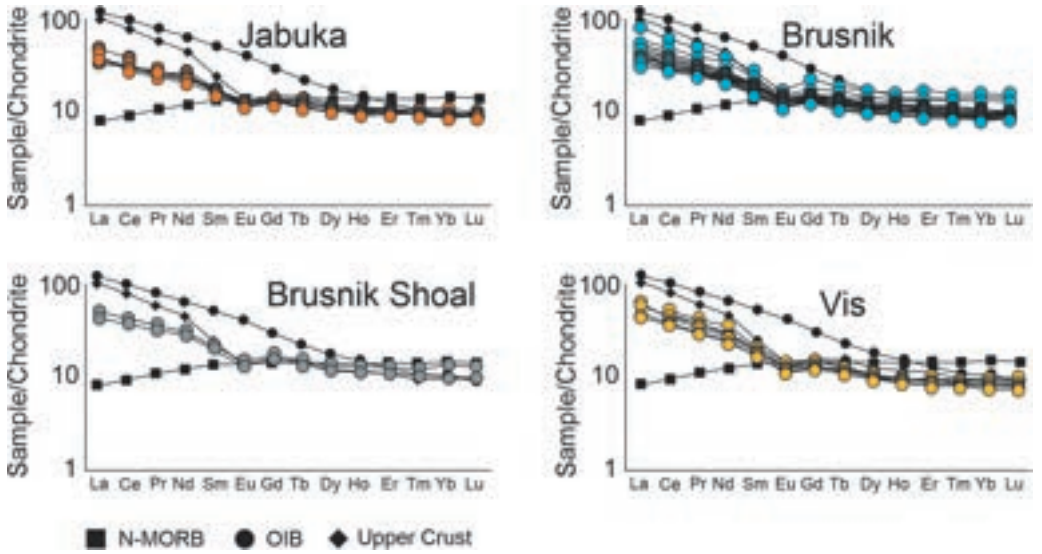

Figure 7. REE patterns of the studied rocks normalized to the chondrite (Boynton 1984).

The primitive mantle (PM, McDonough and Sun 1995) normalized trace element patterns show negative Nb (vs. Th and La) and Ti (vs. Sm and Gd) anomalies and slightly positive ones for Hf (Figure 8; vs. Zr and Sm). Two samples from Jabuka (JA20 and BKA) and one from Brusnik (BR3) show a less pronounced negative Nb anomaly, compared to other rocks from the same islands. The patterns of Figure 8 highlight differences in LILE (Large-Ion Lithophile Elements) and Pb among the islands. Jabuka, Brusnik Shoal and Vis samples show generally quite flat LILE and Th, which are clearly enriched compared to the LREE (except for sample VK21, Vis). Brusnik samples show markedly less enriched LILE and can be divided into two groups, the first showing a flat LILE pattern, similar to the samples from the other Islands but at lower contents, the second Brusnik showing a negative anomaly of Rb relative to Ba, K and Th, similar to VK21 (but at lower values). Finally, most Jabuka and Brusnik samples show a positive Pb anomaly (vs. Ce and Pr), opposite to most Vis samples.

The LREE contents of the AMI samples are different from those of the Upper Crust (UC; Rudnick and Gao. 2003), OIB (Ocean Island Basalt; Sun and McDodough, 1989) and N-MORB (Normal Mid Oceanic Ridge Basalt; McDonough and Sun 1989), even though the pattern of the AMI samples recalls that of the UC. In particular, compared to the UC the studied samples show lower enrichment of LREE ($La/Sm_{CN(AMI)}$ = 2.22–2.96, $La/Sm_{CN(UC)}$ = 4.15) and comparable ratios of MREE and HREE ($Sm/Dy_{CN(AMI)}$ = 1.63, $Sm/Dy_{CN(UC)}$ = 1.99; $Dy/Yb_{CN(AMI)}$ = 1.13, $Dy/Yb_{CN(UC)}$ = 1.27).

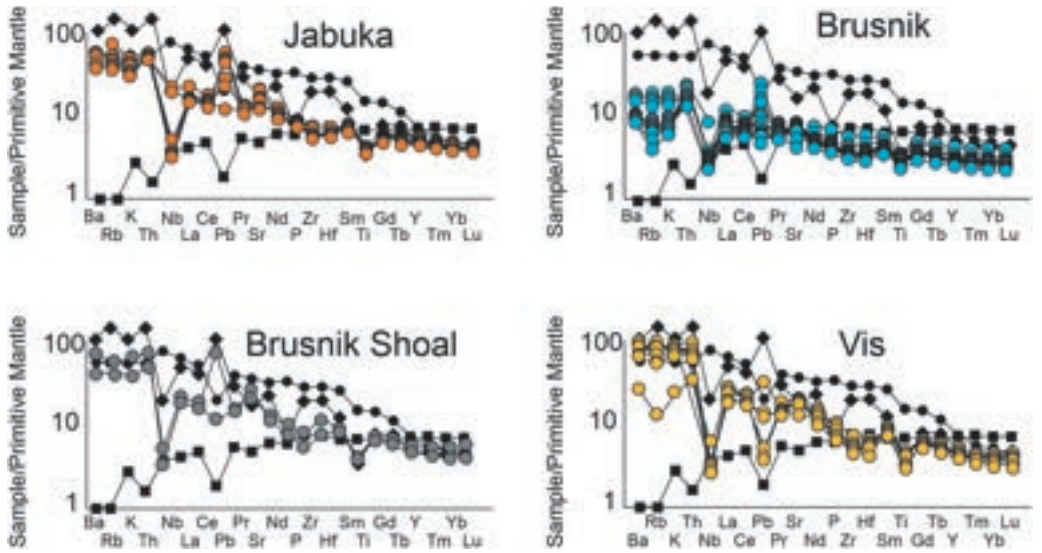

Figure 8. Trace elements diagrams of the studied rocks normalized to the Primitive Mantle (McDonough and Sun 1995). Simbols as Fig. 7.

Sr and Nd isotopic compositions

Whole-rock $^{87}Sr/^{86}Sr$ and $^{143}Nd/^{144}Nd$ isotopic ratios were measured on five representative samples. Among these, one is from Jabuka (BKA), two from Brusnik (BR3 and BK7) and two from Vis (VK16a and VK16b) (Supp. Tab 4). The initial isotopic values, here indicated as $^{87}Sr/^{86}Sr_i$ and $^{143}Nd/^{144}Nd_i$ are corrected for an age of 227 Ma. The less enriched sample is BR3 from Brusnik [$^{87}Sr/^{86}Sr_i$ = 0.704615 (24), $^{143}Nd/^{144}Nd_i$ = 0.512551(24) and εNd = 4.1], which plots close to the field of the anorogenic Triassic basalts of Mt. Kalnik (Figure 9). On the contrary, the most enriched samples are those from Vis [$^{87}Sr/^{86}Sr_i$ = 0.705571(22)-0.705647(6), $^{143}Nd/^{144}Nd_i$ = 0.512152(23)-0.512185(6) and εNd = −3.1 – −3.7]. These rocks from Vis as well as two samples from Jabuka and Brusnik (BKA and BK7: $^{87}Sr/^{86}Sr_i$ 0.705086(19) and 0.705076(6), $^{143}Nd/^{144}Nd_i$ 0.512359(28) and 0.512311(6), εNd 0.33 and −0.60, respectively; Supp. Table A4) fall close to the Triassic magmatic rocks from the Dolomites. The AMI samples in Figure 9 seem to form a linear trend that parallels the Mantle Array (the cluster that correlates the Sr-Nd isotopic data of MORB, OIB and CFB as defined by De Paolo and Wasserburg 1979), but is shifted towards higher $^{87}Sr/^{86}Sr_i$ values.

Discussion

Age of the Adriatic Island magmatism

The geochronological data obtained in this work contribute to the definition of the age of the AMI, particularly the plagioclase $^{40}Ar/^{39}Ar$ age of 227 ± 5 Ma for Jabuka Island. However, it should be considered that both $^{40}Ar/^{39}Ar$ mini-plateau ages for the AMI are not very robust and should be considered with caution. The disturbed spectra for both samples and the low $^{37}Ar/^{39}Ar$ possibly indicate that the apparent ages were affected by the alteration of the analysed feldspars. In particular, the feldspars of the Brusnik sample BR3 may have been significantly affected by the presence of a K-rich secondary mineral, e.g. sericite. A recent study shows that just a few percent of sericite in the feldspar separate can significantly alter the $^{40}Ar/^{39}Ar$ age (Jiang et al. 2021). Therefore, the apparent age of BR3 (219.5 ± 2.5 Ma) is clearly a minimum age for the crystallization of this sample. Considering its relatively higher

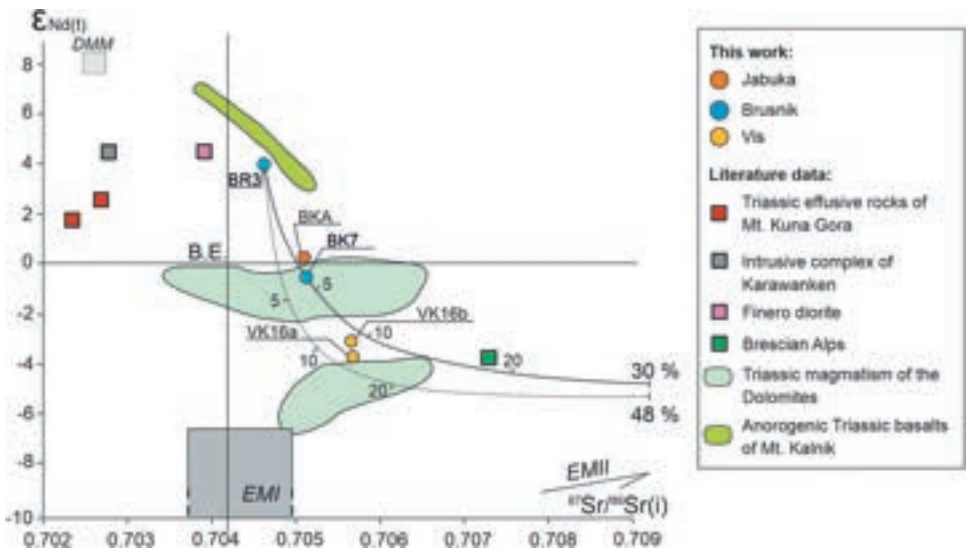

Figure 9. Initial (227 Ma) $^{87}Sr/^{86}Sr_i$ and $\varepsilon Nd_{(t)}$ values of the selected samples (BKA, BR3, BK7, VK16a and VK16b). The Triassic samples from Mt. Kuna Gora (Slovenec and Šegvić 2021), Karawanken (sample 08EK18 from Eisenkappel; Miller et al. 2011), Finero (diorite sample Fi90; Lu et al. 1997a), Southern Alps (Casetta et al. 2019; Lustrino et al. 2019; De Min et al. 2020), Monzoni Mts (Bonadiman et al. 1994), Brescian Prealps (sample CB5; Cassinis et al. 2008) and Mt. Kalnik (samples Kb6 and Vsk207a; Slovenec et al. 2011) have been plotted for comparison. The two lines represent the EC-AFC model calculated considering BR3 sample as parental composition and a cornubianitic metapelite xenolith (black line) and a migmatitic xenolith as contaminants (dotted line; crustal xenolith compositions from Sassi et al. 2020). The isotopic compositions of both contaminants are recalculated at 230 Ma. Depleted MORB Mantle (DMM; light grey shaded fields) and Enriched Mantle I and Enriched Mantle II (EMI and EMII) end-members were calculated for an age of 230 Ma using the isotopic values from Workman and Hart (2005; average DMM) and Hart and Zindler (1989), respectively. The trace element concentration of the mantle end-members are from Workman and Hart (2005) for DMM and from Sun and McDonough (1989) for EMI and EMII. The Bulk Earth (BE) isotopic composition was recalculated at 230 Ma using elemental compositions of Sm and Nd from the recommended chondrite (Boynton 1984) and Rb and Sr from the primitive mantle (PM) of McDonough and Sun (1995)

$^{37}Ar/^{39}Ar$, the apparent age of the Jabuka sample BKA (227 ± 5 Ma) may approach the crystallization age of AMI basalts, even if we cannot exclude that this may also be a minimum age.

Further constraints on the age of this magmatism derive from previous studies on the associated sedimentary rocks. For these, palynological data (Koch and Belak 2003) suggest a Ladinian-Norian age, which is consistent with the $^{40}Ar/^{39}Ar$ age for sample BKA. On the contrary, Palinkaš et al. (2010) refer to Permian ages for the AMI, but the precise data and methodology have never been published and, more generally, Permian ages seem not consistent with the local geology and stratigraphy. Therefore, we conclude that the most likely age of AMI is early Norian or Carnian, even if we can not exclude it to be slightly older.

Comparison with triassic magmatism in the adria plate and its borders

The Triassic magmatism of the Croatian Islands is here compared with coeval (or nearly coeval) occurrences cropping out in the Adria Plate (Southern Alps and Brescian Prealps) and at the edge between Tisia and Adria Plates along an extensional setting (Zagorje-Mid-Transdanubian Zone; Figure 1). In particular, trace element contents and Sr-Nd isotopic ratios of several dykes and flows from the Southern Alps (Lustrino et al. 2019; De Min et al. 2020), of the shoshonitic magmas of the Triassic Monzoni intrusive complex (Casetta et al. 2018a, b), of volcanic and sub-volcanic bodies of the Brescian Prealps (Cassinis et al. 2008) and of pyroclastic rocks of the Zagorje-Mid-Transdanubian Zone (Slovenec et al. 2011; Slovenec and Šegvić 2021). The samples of the latter area seem to belong to two different geologic domains; the Mt. Kuna Gora is part of the Southern Alps Unit (Slovenec and Šegvić 2021; Figure 1), while the Kalnik Mts. are located in an extensional area between Adria and Tisia Plates (Slovenec et al. 2011).

The REE of the Dolomite lava flows (De Min et al. 2020) and intrusives (Predazzo Complex; Casetta et al. 2018a, 2018b) show similar features to the AMI samples (Figure 10), e.g. a general LREE enrichment with a steep LREEs slope and a quite flat M/HREE pattern (Figure 10). However, the LREE slope of the Jabuka, Brusnik and Brusnik Shoal samples appear generally slightly less strong (La_{CN}/Sm_{CN} = 2.25–2.41) than those of the Southern Alps magmatism and of Vis (La_{CN}/Sm_{CN} = 2.91 and 2.83, respectively). Similarly, the Triassic tholeiitic samples from the Brescian Prealps and calcalkaline rocks from Mt. Kuna Gora well overlap the patterns of our samples (Figure 10), except for a slightly more accentuated negative Eu anomaly shown by the Brescian samples (Cassinis et al. 2008; Slovenec and Šegvić 2021). The incompatible element patterns show comparable features for the Adriatic Magmatic Islands, the Southern Alps (Casetta et al. 2018a; De Min et al. 2020), and the Brescian Prealps (Cassinis et al. 2008).

On the contrary, the magmatic rocks cropping out at the junction between Adria and Tisia Plates (Mt. Kalnik; Slovenec et al. 2011), and those at the northwesternmost (Finero; Lu et al. 1997) and northeasternmost edge of the Adria Plate (Miller et al. 2011) show clearly distinct trace element patterns compared to AMI samples (Figure 10), but resemble those of OIBs to MORBs (McDonough and Sun 1995).

The $^{143}Nd/^{144}Nd_i$ of most AMI samples show values comparable to those of the Triassic magmatism of the Southern Alps (Cassinis et al. 2008; Casetta et al. 2018b; De Min et al. 2020), while $^{87}Sr/^{86}Sr_i$ values appear slightly enriched (Figure 9). Only BR3 is clearly more depleted (higher Nd and lower Sr isotopic composition) than the Dolomite basalts and intrusives and plots close to the field of the Kalnik Mts. Consistently with their REE

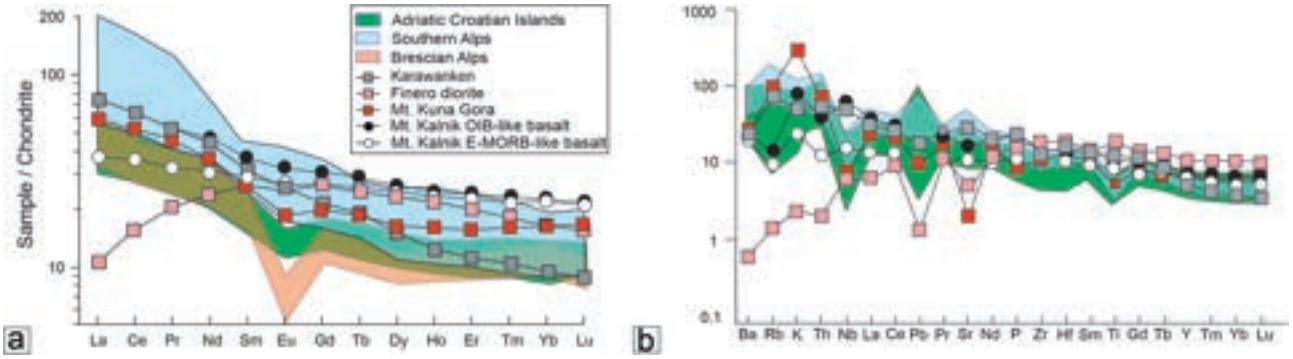

Figure 10. a) REE pattern normalized to the Chondrite (Boynton 1984) and b) trace elements patterns normalized to the Primitive Mantle (McDonough and Sun 1995) of the studied samples and of other Triassic magmatic rocks used for comparison. Literature data as in Figure 9. Sample tskg10 is plotted as representative for Mt. Kuna Gora (Slovenec and Šegvić 2021). The Brescian Prealps (Cassinis *et al*. 2008) are not plotted since trace element data for those rocks are not published.

patterns, Kalnik Mts. samples show quite depleted isotopic compositions.

Magmatic system of the adriatic magmatic islands

Geological and petrographic features suggest that the magmatic occurrences of the AMI probably represent a single magmatic system. The plutonic rocks of Jabuka suggest that the island could be formed by the remnants of the relatively deep intrusion part of the magmatic system, while Brusnik and Brusnik shoal represent a shallow intrusive stage, being mainly composed by sills, and Vis host the erupted products.

The magmatic system has been uplifted by two saline diapirs that probably were in contact during Triassic times. The halokinetic movements were triggered by the Cenozoic Dinaric orogeny (Pikelj et al. 2015). One diapiric body lies under Jabuka Island and the other one extends under Brusnik/Brusnik shoal and outcrops in Vis (Kulušić and Borojević Šostaric 2014; Pikelj et al. 2015). The two tore and uplifted the old buried magmatic complex to different positions, tilting the entire structure.

Considerations on the textural features and zoning of some mineral grains and the application of several mineral-melt equilibrium models (Putirka 2008, 2016; Neave and Putirka 2017) restricted the number of methods to estimate the near-liquidus pressure and temperature of crystallization to the clinopyroxene-melt geothermobarometer. Under the assumption that the whole-rock represents the equilibrium liquid composition, we applied the geobarometer of Neave and Putirka (2017) and the geothermometer (equation 33) of Putirka (2008). However, only one clinopyroxene in sample BK4 shows K_d (Fe-Mg)$^{cpx\text{-}liq}$ and clinopyroxene components compatible with equilibrium (see Putirka 2008). Estimated temperature and pressure for this sample are 1062 ± 20 °C and −0.2 ± 1.4 kbar, where the uncertainties are the model errors as reported in the source papers. Such low pressure is compatible with crystallization in the sill-like body of Brusnik, which is supposed to be the shallow intrusive stage of the magmatism, supporting the petrographic and geological observations.

Crustal, magma-seawater or evaporite contaminations?

The enriched $^{87}Sr/^{86}Sr_i$ and low $^{143}Nd/^{144}Nd_i$ of most AMI rocks suggest a significant contribution from the continental crust. This crustal signature may be related to an open-system differentiation (combined fractionation and crustal assimilation) or to a mantle source enriched by recycled crustal components, as it has been discussed for the Triassic Adriamagmatism from the Southern Alps (Lustrino et al. 2019; De Min et al. 2020).

To evaluate the possible role of crustal contamination processes we applied the Energy-Constrained Assimilation-Fractional Crystallization (EC-AFC) model of Spera and Bohrson (2001). The input data are reported in the Supp. Table A5. As parental magma we selected the most depleted of the AMI samples (BR3: $^{143}Nd/^{144}Nd_i$ = 0.51255, $^{87}Sr/^{86}Sr_i$ = 0.71462), while the considered contaminants are Permian crustal xenoliths from different depths of the Adria Plate continental crust (Sassi et al. 2020), i.e. migmatitic ($^{143}Nd/^{144}Nd_i$ = 0.51179 and $^{87}Sr/^{86}Sr_i$ = 0.71448) and cornubianitic metapelite xenoliths ($^{143}Nd/^{144}Nd_i$ = 0.51180 and $^{87}Sr/^{86}Sr_i$ = 0.72527; all data recalculated to 230 Ma). The results of the EC-AFC simulation show that assimilation of the cornubianitic metapelite best reproduces the evolution of the AMI samples as well as those from the Brescian Prealps (Cassinis et al. 2008). The amount of crustal assimilation needed to reach from BR3 the most enriched AMI samples is ca. 5–10 wt.%, with ca. 53–59 wt.% of fractionation, while to approach the Brescian Prealps sample ($^{143}Nd/^{144}Nd_i$ = 0.51215 and $^{87}Sr/^{86}Sr_i$ = 0.70729; Cassinis et al. 2008) ca. 16 wt.% assimilation and 65 wt.% fractionation is estimated. Assimilation of the cornubianite (SiO_2 = 51.75 wt.%) is not expected to significantly increase the silica content of the contaminated AMI samples. However, the calculated amount of fractionation may not be reasonable as BR3 and the other studied AMI samples are similarly evolved, i.e. have similar major element composition. It may be suggested that the enriched isotopic compositions may be due to an assimilation process similar to that modelled, but with a more primitive magma as starting composition.

Notably, Brusnik and Vis samples show a linear positive correlation between Na_2O content and Sr isotopic ratio (Figure 11), suggesting that the magmas interacted with seawater or with the evaporites (or both). Alteration does not seem to be too severe as indicated by the moderate loss of ignition (L.O.I.) that spans from 0.8 (B5) to 2.3 wt.% (VK16B) (Supp. Table A1). The Brusnik and Vis samples point to a contaminant that may be represented by lagoonal evaporites (Na_2O ca. 6 wt.%, Bahadori et al. 2011, p. $87Sr/^{86}Sr_i$ of Triassic seawater = 0.7077; Onoue et al. 2018). This agrees with previous studies that suggested a tidal flat environment deposition for the evaporite outcropping in Vis (Koch and Belak 2003). The analysed Jabuka sample does not plot on the same trend as the other AMI samples, but it is enriched in Na_2O. It could suggest that BKA was contaminated by a Na-enriched evaporite like those from sabkhas (Na_2O = 13.10 wt. %; Bahadori et al. (2011). However, the evaporite that lies under Jabuka has not

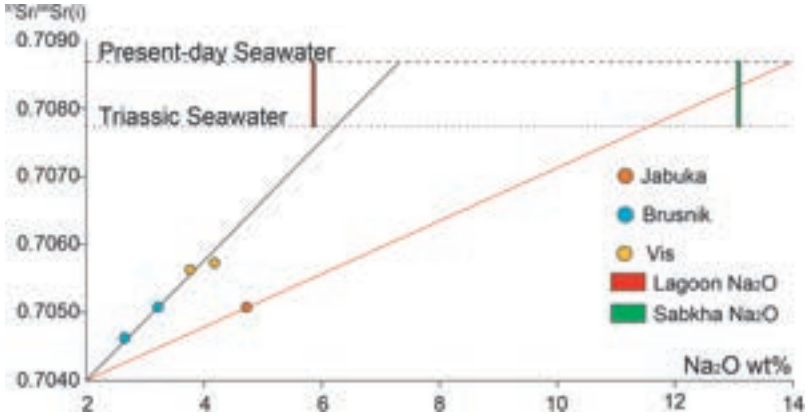

Figure 11. Variation of Na_2O (wt.%) vs. $^{87}Sr/^{86}Sr_i$ of the analysed samples. The black full line represents the linear trend obtained from the interpolation of the Brusnik and Vis samples. Notably, the intersection between the interpolation line and the ordinate axis correspond to an $^{87}Sr/^{86}Sr_i$ value comparable to the less altered samples of the Dolomites ($^{87}Sr/^{86}Sr_i \sim 0.7041$; De Min *et al*. 2020). The red line represents a hypothetical line built by linking the Jabuka sample to the intersection between the projection of the previously obtained linear trend (black line) and the ordinate axis, here chosen as hypothetical representative value of a common unaltered sample. The dotted line represents the Triassic seawater $^{87}Sr/^{86}Sr_i$ value ($^{87}Sr/^{86}Sr_i = 0.7077$) that has been calculated using as representative end-member a median $^{87}Sr/^{86}Sr$ value of Norian Radiolarian thin-shelled bivalve mudstone-wackestone outcropping in Pizzo Mondello (Italy; Onoue et al. 2018) and coeval conodonts for the Nd isotopic ratio (Shaw and Wasserburg 1985). The dashed line indicates the present-day $^{87}Sr/^{86}Sr_i$ seawater ($^{87}Sr/^{86}Sr_i = 0.708659$; McCulloch and De Dekker 1989). Red and green boxes represent the lagoon and sabkha Na_2O content suggested by Bahadori et al. (2011), respectively.

been directly studied and is only known from geophysical surveys.

Mantle source

We used the $(Gd/Yb)_{CN}$ vs $(La/Yb)_{CN}$ diagram (Figure 12a) to constrain the partial melting degree, the possible presence of spinel and/or garnet in the residual source rock and to investigate if a phlogopite-bearing peridotite could have played a role in the genesis of the relatively K-rich AMI magmas. In the diagram, there are two series of isopleths and magma mixing lines, one representing the mixing between spinel and garnet peridotite melting curves (black in the diagram, Figure 12a), while the second considers the mixing between a spinel peridotite and a spinel-phlogopite harzburgite (red in the diagram, Fig, 12a).

The investigated samples fall entirely in an area between 1 and 5% of partial melting and under the 80% – 60% of spinel content isopleth in the garnet-spinel (black lines in Figure 12a) and spinel-spinel + phlogopite models (red curves), respectively (Figure 12a). The first isopleth represents the ratio of spinel/garnet in the mantle source and suggests a rather shallow melting depth (low or absent residual garnet). The second ratio, which indicates the relative amount of phlogopite in the mantle source, suggests that the mantle source may have been partly metasomatized and contained some phlogopite. The basalts of the Dolomites (De Min et al. 2020) partially plot out of the spinel-spinel + phlogopite models, showing generally lower partial melting degrees, a higher melting pressure (more garnet in the mantle source), and possibly a more enriched source (higher amounts of phlogopite). The shallowing of the melting depth from northern (Dolomites) to southern Adria (AMI) possibly could be explained by progressive southward lithospheric thinning during Triassic times as suggested by De Min et al. (2020). The few samples of the ZMTDZ (Slovenec et al. 2011) that show less MORB-like features plot in the same area of the AMI samples or very close to them, suggesting a similar dominantly spinel peridotite source.

The tectonomagmatic diagrams in Figure 12b (Pearce et al. 2021), 12C (Pearce and Cann 1973) and 12D (Wood 1980) show that the basalts of the Dolomites (De Min et al. 2020), Mt. Kuna Gora (Slovenec and Šegvić 2021) and AMI samples (this study), thus all the here considered Triassic magmas outcropping in the Adria Plate, mainly fall close to each other. More specifically, in Figure 12c they plot in the B and C fields that represent MORB + VAB and VAB affinities (MORB = Mid Ocean Ridge Basalt; VAB = Volcanic Arc Basalt), respectively, while they are grouped in the calc-alkaline arc-related effusive and pyroclastic rocks field in Figure 12d. Finally, in the diagram (Figure 12b) recently introduced by Pearce et al. (2021), the Triassic magmas outcropping in the Adria Plate plot along the IAB field (Island Arc Basalts; Figure 12b). The three tectonomagmatic diagrams appear in agreement and suggest a significant crustal input as would be consistent with the isotopic

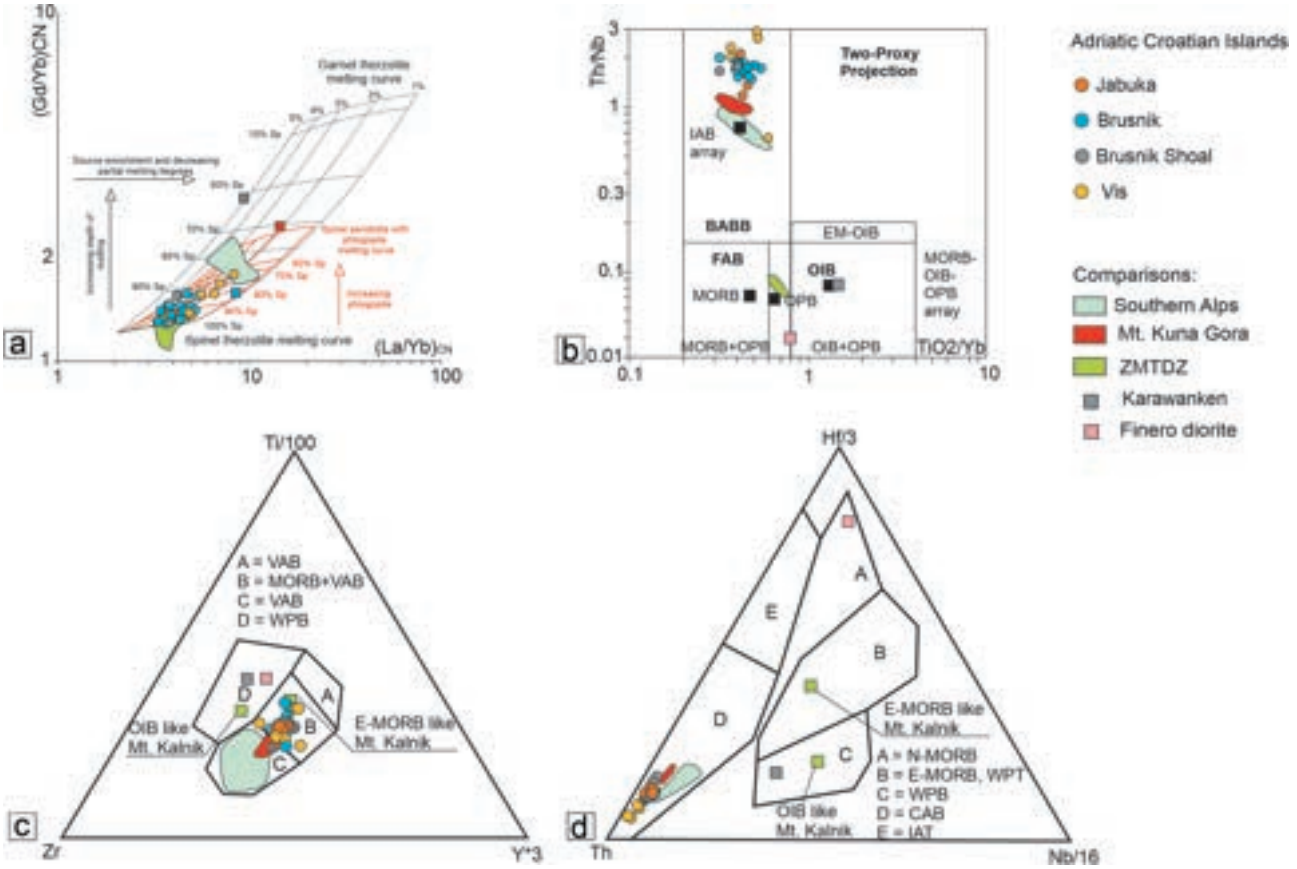

Figure 12. a) Diagram representing a fractional partial melting model using REE systematics. On the top of the diagram, the percentages represent the partial melting degrees, while those on the sides represent the spinel-garnet ratio in the source mineralogy (black) and spinel peridotite vs spinel+phlogopite peridotite mixing ratio (red). The red and blue square represent the cornubianite metapelitic and migmatitic xenoliths (Sassi et al. 2020). Calculated partial melting curves are drawn assuming fractional melting of garnet-spinel peridotite and spinel + phlogopite harzburgite. Modal mineral composition of garnet peridotite (Ol = 0.578, OPX = 0.27, Cpx = 0.119 and Gt = 0.115) as suggested by McKenzie and O'Nions (1991), spinel peridotites as suggested by McDonough and Sun (1995) (Ol = 0.5, Opx = 0.22, Cpx = 0.19 and Sp = 0.03) and spinel-phlogopite hazburgite (Ol = 0.73, Opx = 0.21, Cpx = 0.037, Sp = 0.001 ad Phl = 0.019) as suggested by Bonadiman et al. (2021). The partition coefficients used in this model are from McKenzie and O'Nions (1991) and Adam and Green (2006). The Primitive Mantle values (McDonough and Sun 1995) have been chosen as starting composition of the spinel peridotite, the E-MORB (McDonough and Sun 1995) one for the garnet peridotite and the values of Bonadiman et al. (2021) for the composition of spinel-phlogopite harzburgite. Ol: olivine, Opx: orthopyroxene, Cpx: clinopyroxene, Gt: garnet, Sp: spinel and Phl: phlogopite. b) Tectonomagmatic diagram suggested by Pearce et al. (2021, modified), IAB = Island Arc basalt, BABB = Back-Arc Basin Basalt, FAB = Fore-Arc Basalt, MORB = Mid-Ocean Ridge Basalt, OPB = Oceanic Plateau Basalt, EM = Enriched Mantle and OIB = Ocean Island Basalt. c) Tectonomagmatic diagram suggested by Pearce and Cann (1973), VAB = Volcanic Arc Basalt, MORB = Mid-Ocean Ridge Basalt, WPB = Within Plate Basalts. d) Tectonomagmatic diagram suggested by Wood (1980), N-MORB = Normal Mid-Ocean Ridge Basalt, E-MORB = Enriched Mid-Ocean Ridge Basalt, WPT = Within-Plate Tholeiites, WPB = Within Plate Basalts, CAB = Calcalkaline Basalts and IAT = Island Arc Tholeiites.

compositions of the AMI rocks (Figure 9). In contrast, the ZMTDZ (Slovenec et al. 2011), the diorite from the external gabbro unit of the Finero complex (Lu et al. 1997), and Eisenkappel samples (Miller et al. 2011) do not show a subduction signature and plot in the anorogenic field (Figure 12b, 12c and 12d). These latter Triassic occurrences are located at the edge of the Adria Plate (i.e. Finero) or beyond its northernmost margin. Notably, the lack of the anorogenic features in Finero implies that the upper part of the mantle under the Ivrea Verbano Zone has not been influenced by past subductions, testifying the complex geology of the Area.

Figure 13 identifies three broad trends, which seem in agreement with Figure 12a. The AMI samples show quite low $(Sm/Yb)_N$ (1.91 to 2.48) and a high range of $(K/Nb)_N$ (1.65 to 31.98), which is consistent with a small presence of garnet in the source and an enrichment in K due to the melting of phlogopite in the source at shallow depths. Notably, the large range of $(K/Nb)_N$ values is mainly due to the different K content in the samples

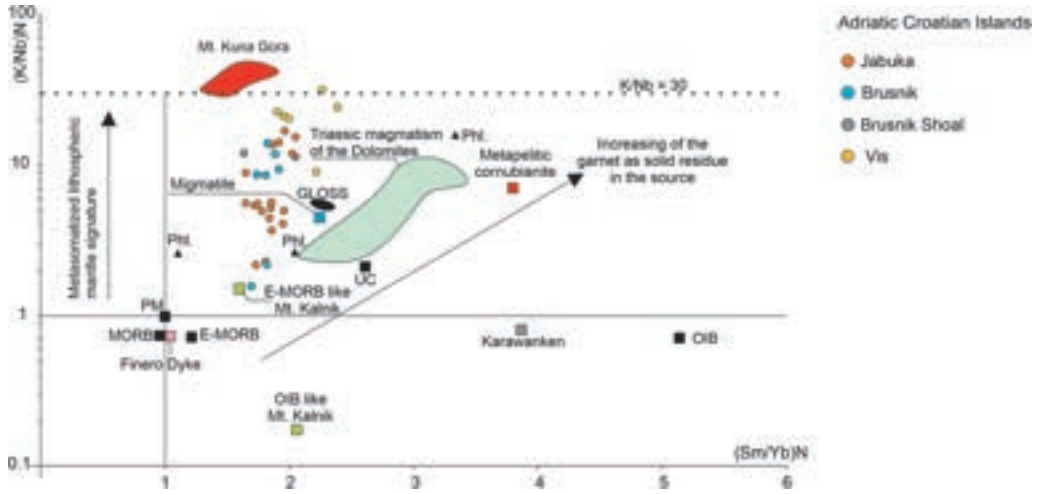

Figure 13. $(K/Nb)_N$ vs. $(Sm/Yb)_N$ diagram of the investigated samples together with the Triassic magmatism outcropping in the Adria Plate and its borders. The black triangles are the phlogopite of the Finero Complex studied by Giovanardi et al. (2014), the red and blue square represent the cornubianite metapelitic and migmatitic xenoliths (Sassi et al. 2020), while the dotted line represents the smallest $(K/Nb)_N$ ratio of the Finero phlogopite studied by Zanetti et al. (1999). All the data are normalized to the Primitive Mantle (McDonough and Sun 1995). MORB (Normal Mid Ocean Ridge Basalt), E-MORB (Enriched- Mid Ocean Ridge Basalt), OIB (Ocean Island Basalt) and PM (Primitive mantle) values are after Sun and McDonough (1989) and McDonough and Sun (1995), GLOSS (Global Subducting Sediments) values are after Plank (2014) and UC (Upper Crust) values are after Rudnick and Gao. (2003). The green areas represent the Mt. Kalnik Triassic magmatic rocks (Slovenec et al. 2011), the other symbols and literature data as Figure 9

rather that to a difference in Nb (Supp. Table A1). The migmatite studied by Sassi et al. (2020) plot near the GLOSS composition (Plank 2014), while the cornubianite metapelite xenolith shows higher $(K/Nb)_N$ and $(Sm/Yb)_N$ values (migmatite = 7.03 and 3.78, respectively; cornubianite = 4.56 and 2.24, respectively). Both crustal xenoliths do not show a very high $(K/Nb)_N$, suggesting that both these rocks are not the main cause of the $(K/Nb)_N$ enrichment of the AMI samples. Considering that the AMI samples show generally low values of loss on ignition (L.O.I; Supp. Table A1), which suggest small degree of alteration, and that similar magmatic rocks found in the Dolomites (with similar of alteration) are generally considered as shoshonites (e.g. Casetta et al. 2019, 2021; Lustrino et al. 2019), this could imply that the main reason of the high $(K/Nb)_N$ should be due to melting of a metasomatized mantle peridotite, possibly with phlogopite in the source.

The Triassic basaltic rocks of the Dolomites (De Min et al. 2020) show higher $(Sm/Yb)_N$ at comparable $(K/Nb)_N$ and a general positive correlation between the two ratios ($(K/Nb)_N$ = 2.38–11.06 and $(Sm/Yb)_N$ = 2.09–3.42). This would indicate a higher content of garnet (higher depth of mantle melting) and an overall smaller presence of phlogopite in the mantle source compared to the AMI magmas. Finally, most Triassic magmatic rocks that outcrop outside the Adria Plate show $(K/Nb)_N < 1$ and plot between the MORB and OIB end-members, with the exception of the E-MORB-like sample from Mt. Kalnik ($(K/Nb)_N$ = 1.51 and $(Sm/Yb)_N$ = 1.59; Slovenec et al. 2011) that plots between the E-MORB and the basaltic suite of the Dolomites.

Casetta et al. (2019) suggested that Norian lamprophyric dykes from Predazzo could represent the markers of the shift from orogenic-like to anorogenic magmatism in the Southern Alps, due to a progressive depletion of the mantle source. However, the apparently coeval magmatism outcropping in the Brescian Prealps (part of the Southern Alps Unit) does show a clear subduction signature, similar to the Ladinian magmatism of the Dolomites. Furthermore, the data presented in this work show that also the Mid-Upper Triassic AMI samples have an apparent subduction fingerprint, which is even stronger than those shown by the magmatic rocks outcropping in the northern Adria (Dolomites and Brescian Prealps). These discrepancies could be justified considering one or both of these two assumptions:

- first, the $^{40}Ar/^{39}Ar$ ages of the AMI and of the Brescian Prealps (Cassinis et al. 2008) are probably minimum ages, and it could be possible that their magmatic crystallization ages are somewhat older, i.e. Ladinian instead of Carnian/Norian;
- second, the mantle source composition varies under Adria being more depleted for the Norian Predazzo lamprophyres than for the ca. coeval AMI and Brescian magmatism. .

However, the geochemical and isotopic differences between the Southern Alps lamprophyres and the other Carnian-Norian Triassic Adria magmas could be due to a deeper melting for the lamprophyres compared to the other Triassic magmas (Casetta et al. 2019; De Min et al. 2020). If this hypothesis is correct, it would imply that the deeper part of the upper mantle was less influenced by ancient subduction under the Adria Plate.

Geodynamic implications

In Figure 14 the main Triassic magmatism occurrences in the Adria Plate and neighbouring areas are shown together with a simplified incompatible elements pattern which reflects the three main geochemical features of the Triassic Adria magmatism: the variable amount of LILE content, the negative Nb anomaly (identified by the K/Nb_{PM} ratio) and the generally flat HFSE (High Field Strength Elements) pattern (cf. Figure 10). The variations of these geochemical features appear to be related to the position of the outcrops in relation to the Adria Plate. More specifically, the magmatic rocks at the edge of the Adria Plate (Finero, Zagorje-Mid-Transdanubian Zone and Karawanken Area; Lu et al. 1997; Miller et al. 2011; Slovenec et al. 2011) show no subduction features, i.e. they lack a negative Nb anomaly ($K/Nb_{PM(Finero)}$ = 0.38; $K/Nb_{PM(Karawanken)}$ = 0.93; $K/Nb_{PM(Zagorje\text{-}Mid\text{-}Transdanubian)}$ = 1.32–1.51) and have relatively low LILE contents. On the contrary, basaltic magmas from the inner portions of the Adria Plate show pronounced subduction traits (mean $K/Nb_{PM(Kuna\ Gora)}$ = 38.6; $K/Nb_{PM(Dolomites)}$ = 7.4 (mean); $K/Nb_{PM(AMI)}$ = 10.5).

The common presence of the inherited subduction signature in the Triassic magmatism outcropping in the Adria Plate suggests that an old (pre-Triassic) subduction affected the entire Plate, with the exception of the Ivrea Verbano Area, and that it modified the chemical nature of the upper part of the mantle beneath the Adria Plate. The lack of subduction characteristics in the coeval magmatism that outcrops just outside the Adria Plate supports the idea that extensional geodynamics acted along its borders. Furthermore, the presence of both subduction-like and anorogenic magmatism suggests that the extension triggered the melting of portions of mantle related to both the Adria Plate and the territories that occur north of the Intra Pangea Dextral Shear (IPDS) (Figure 14, modified after Schettino and Turco 2011). These features suggest that past subduction(s) merged towards the central part of Adria and that the Intra

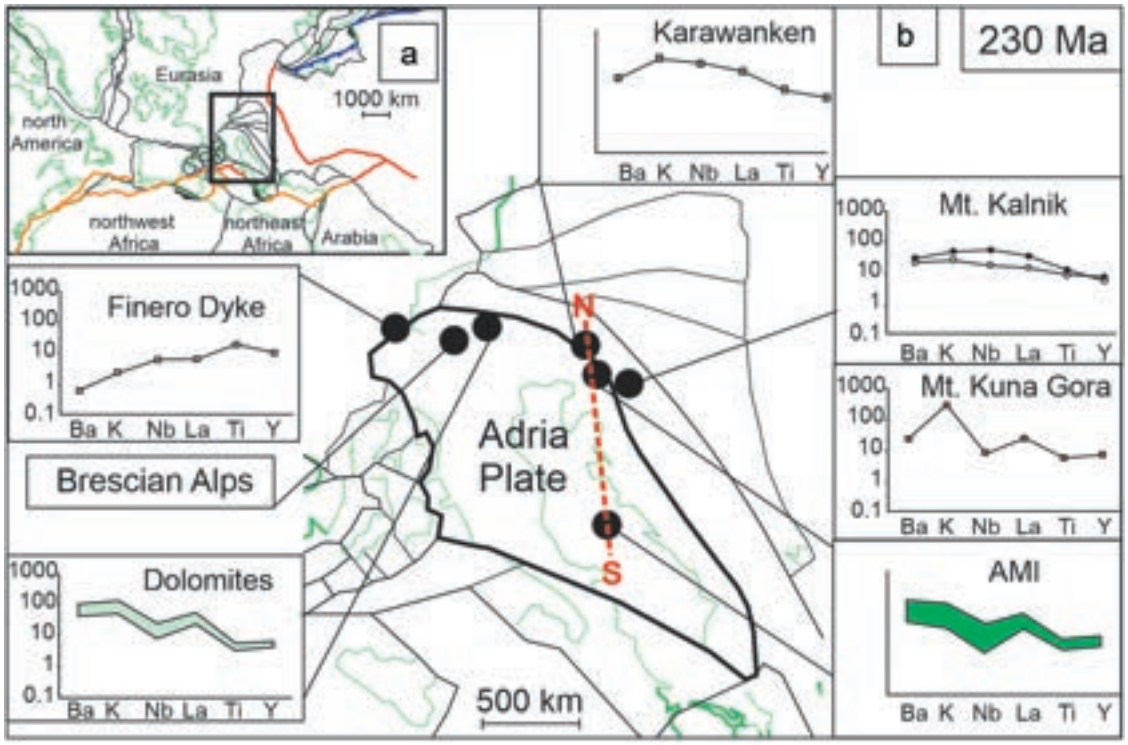

Figure 14. a) Geological sketch representing the Adria Plate position in the Triassic (after Schettino and Turco 2011; De Min et al. 2020). b) Larger view of the Adria plate position at 230 Ma following the reconstruction of Schettino and Turco (2011), showing the main Triassic magmatic outcrops in the Adria Plate and neighbouring areas. The Brescian Prealps trace element diagram is not shown since those data were not published In Cassinis et al. (2008). The N-S line represents the profile that has been considered for creating the model in Figure 15

Pangea Dextral Shear did not continue along the southern margin of the Adria plate as suggested by Schettino and Turco (2011), but along the present-day Periadriatic line and the external Dinarides.

In Figure 15 we propose a sketch model that reassumes the geodynamic evolution of the Adria Plate and the nearby Karawanken area in the Upper Triassic. During the Carnian, extensional forces that acted along the Plate margin (Periadriatic Line) stretched and thinned the lithosphere, triggering an asthenospheric upwelling (Figure 15a). The melting area interested both the European and Adria Plates mantle, which probably were located north and south of the Periadriatic Line, respectively (Figure 15a). The resulting magmatism that occurred in the Karawanken and Mt. Kuna Gora Areas show anorogenic and subduction signatures, respectively, reflecting the different nature of the two lithospheric mantles. In the Norian, new extensional events occurred along the margins of the Adria Plate, further thinning the lithosphere and triggering a new pulse of asthenospheric upwelling (Figure 15b). Near the Periadriatic Line, the upwelling acted only under the European Plate lithospheric mantle and triggered a new magmatic event (at least) in the Karawanken, while in the south it generated the AMI magmatism, suggesting that the Adriatic islands were quite near to the margin of the Adria Plate (Figure 15b).

Conclusions

The magmatism of the Adriatic Magmatic Islands is part of the Triassic magmatic pulse that possibly occurred during the Mid-Upper Triassic in the Adria Plate. The samples show textures that could represent a magmatic sequence, which starts in Jabuka with gabbroic rocks and finishes in Vis with volcanics, suggesting that the islands were formerly a unique complex. The EC-AFC model well reproduces the trend of the AMI samples and of the coeval Brescian Prealps magmatic rocks, supporting a common parent melt and crustal contaminant, which could correspond to cornubianitic metapelites. Furthermore, the correlation between the Na_2O content and $^{87}Sr/^{86}Sr_i$ values of the AMI samples suggests contamination with the nearby evaporites formed

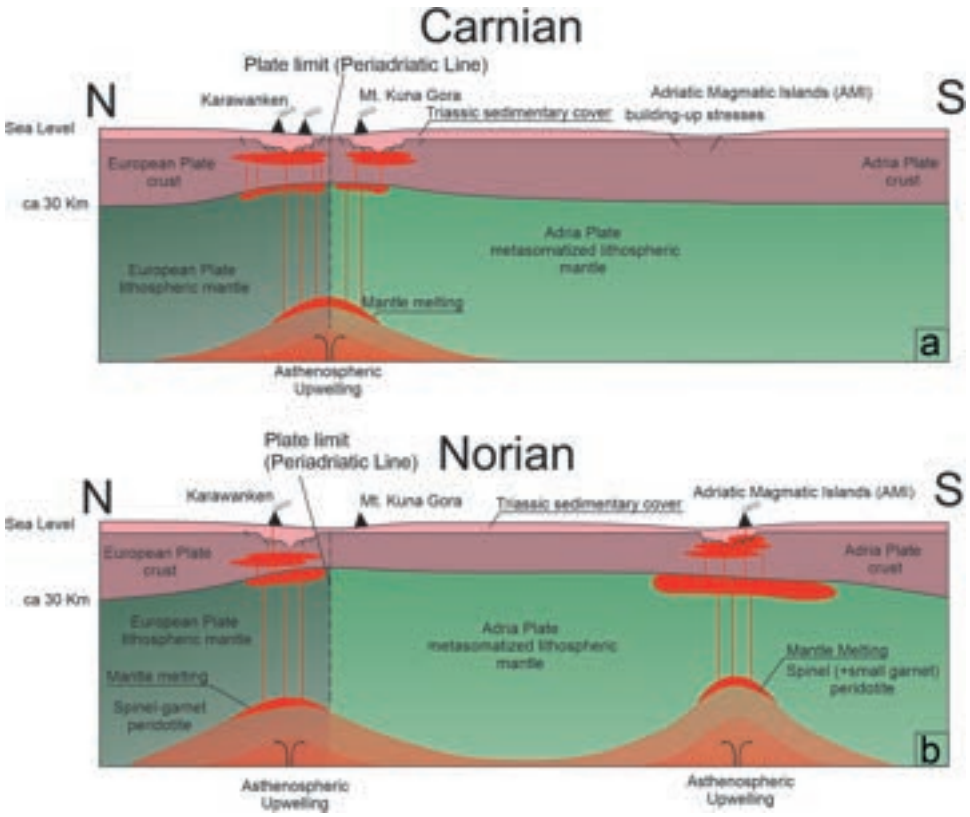

Figure 15. Hypothetical schematic geodynamic evolution model of the Karawanken (European Plate), Mt. Kuna Gora (Adria Plate) and AMI (Adria Plate) along the N-S line (Figure 14) for the Carnian (a) and Norian (b) ages. In (a) the extension and the resulting lithospheric thinning occurred mainly along the Periadriatic Line, generating an asthenospheric upwelling. In (b) a second series of extensional movements further thinned the lithosphere, generating an asthenospheric upwelling along the Periadriatic line and the margin of the Adria Plate, triggering the second pulse of the Karawanken and the AMI magmatism. Depths of magmatic processes in the mantle are not well constrained, the vertical scale therefore shows only the inferred values.

in a sabkha-like (Jabuka Island) or in a lagoon-like environment (Brusnik and Vis). The evaporitic diapirs contributed to the exhumation of the magmatic rocks. The magmatic samples show geochemical characteristics compatible with melting of a variably metasomatized shallow mantle source, possibly a spinel peridotite with a small garnet component and variable phlogopite contents. The comparison made with the apparently slightly older or coeval Southern Alps basalts suggests that the melting could have occurred during lithospheric thinning, as has been invoked by De Min et al. (2020). Finally, the apparent subduction signature of the samples could mainly be related to the nature of the upper mantle under the Adria Plate that previously has been enriched by one or more pre-Mesozoic subductions events.

Acknowledgments

The authors thank Dr. Mathieu Benoit of the GET-OMP (Toulouse, France) for the Sr-Nd isotopic analyses and the technician Lorenzo Furlan (University of Trieste, Italy) for preparing the thin sections. We also thank the Editor Prof. J. Stern for the precious suggestions and helpfulness, as well as Dr. F. Casetta and the anonymous reviewer 2 for the constructive reviews and insightful questions. Financial support was provided by PRIN-2017 (Italian PRIN 20178LPCP to AM and ADM).

Disclosure statement

The authors declare that they have no known competing financial interests or personal relationships that could have appeared to influence the work reported in this paper.

Funding

This work was supported by the PRIN-2017 (Italian PRIN to AM and ADM) [20178LPCP].

Partecipation

Angelo De Min designed the study; Matteo Velicogna and Angelo De Min wrote the paper with the contribution of all authors; Angelo De Min, Matteo Velicogna, Marko Kudrna Prašek and Dražen Balen conducted the petrographic, mineralogical and the geochemical analyses; Angelo De Min and Marko Kudrna Prašek conducted the field activity; Matteo Velicogna, Angelo De Min, Marko Kudrna Prašek and Valentina Brombin conducted the isotopic analyses; Fred Jourdan and Paul Renne did the $^{40}Ar/^{39}Ar$ analyses; Matteo Velicogna, Angelo De Min, Luca Ziberna and Andrea Marzoli contributed to final interpretation of the data with the help of the other authors.

References

Adam, J., and Green, T., 2006, Trace element partitioning between mica-and amphibole-bearing garnet lherzolite and hydrous basanitic melt: 1. Experimental results and the investigation of controls on partitioning behaviour: Contributions to Mineralogy and Petrology, v. 152, no. 1, p. 1–17. 10.1007/s00410-006-0085-4

Arculus, R.J., 2003, Use and abuse of the terms calcalkaline and calcalkalic: Journal of Petrology, v. 44, no. 5, p. 929–935.10.1093/petrology/44.5.929

Bahadori, A., Carranza, E.J.M., and Soleimani, B., 2011, Geochemical analysis of evaporite sedimentation in the gachsaran formation, zeloi oil field, southwest Iran: Journal of Geochemical Exploration, v. 111, no. 3, p. 97–112.10.1016/j.gexplo.2011.02.007

Balogh, K., Colantoni, P., Guerrera, F., Majer, V., Ravasz-Baranyai, L., Renzulli, A., Veneri, F., and Alberini, C., 1994, The medium-sized gabbro of the Jabuka Islet (Scoglio del Pomo, Adriatic Sea): Giornale di Geologia, ser. 3a, v. 56, no. 2. p. 13–25

Beccaluva, L., Coltorti, M., Saccani, E., Siena, F., and Zeda, O., 2005, Triassic magmatism and Jurassic ophiolites at the margins of the Adria Plate: CROP PROJECT: Deep seismic exploration of the central mediterranean and Italy Finetti, I. R., Elsevier:Amsterdam. 607–621

Bianchini, G., Natali, C., Shibata, T., and Yoshikawa, M., 2018, Basic dykes crosscutting the crystalline basement of valsugana (Italy): New evidence of early triassic volcanism in the Southern Alps: Tectonics, v. 37, no. 7, p. 2080–2093.10.1029/2017TC004950

Bohrson, W.A., and Spera, F.J., 2001, Energy-constrained open-system magmatic processes II: Application of energy-constrained assimilation–fractional crystallization (EC-AFC) model to magmatic systems: Journal of Petrology, v. 42, no. 5, p. 1019–1041. 10.1093/petrology/42.5.1019

Bonadiman, C., Brombin, V., Andreozzi, G.B., Benna, P., Coltorti, M., Curetti, N., Faccini, B., Merli, M., Pelorosso, B., Stagno, V., Tesauro, M., and Pavese, A., 2021, Phlogopite-pargasite coexistence in an oxygen reduced spinel-peridotite ambient: Scientific Reports, v. 11, no. 1, p. 1–17. 10.1038/s41598-021-90844-w

Bonadiman, C., Coltorti, M., and Siena, F., 1994, Petrogenesis and T-fO2 estimates of Mt. Monzoni complex (Central Dolomites, Southern Alps): A Triassic shoshonitic intrusion in a transcurrent geodynamic setting: European Journal of Mineralogy, v. 6, no. 6, p. 943–966.10.1127/ejm/6/6/0943

Bortolotti, V., and Principi, G., 2005, Tethyan ophiolites and pangea break-up: The Island Arc, v. 14, no. 4, p. 442–470.10.1111/j.1440-1738.2005.00478.x

Boscaini, A., Marzoli, A., Davies, J.F., Chiaradia, M., Bertrand, H., Zanetti, A., Visonà, D., De Min, A., and Jourdan, F., 2020, Permian post-collisional basic magmatism from corsica to the southeastern Alps: Lithos, v. 376, p. 105733. 10.1016/j.lithos.2020.105733

Boynton, W.V., 1984, Geochemistry of the rare earth elements: Meteorite studies: Rare Element Geochemistry Henderson, P., Amsterdam: Elsevier. 63–114.

Brkić, M., Špoljarič, D., and Makovinovič, D., 2011, Geomagnetska i GNSS izmjera vrha otočića Jabuke: Geodetski list, v. 65, no. 883, p. 195–204

Casetta, F., Coltorti, M., Ickert, R.B., Bonadiman, C., Giacomoni, P.P., and Ntaflos, T., 2018a, Intrusion of

shoshonitic magmas at shallow crustal depth: T–P path, H2O estimates, and AFC modeling of the middle triassic predazzo intrusive complex (Southern Alps, Italy): Contributions to Mineralogy and Petrology, v. 173, no. 7, p. 1–27.10.1007/s00410-018-1483-0

Casetta, F., Coltorti, M., and Marocchino, E., 2018b, Petrological evolution of the middle triassic predazzo intrusive complex, Italian Alps: International Geology Review, v. 60, no. 8, p. 977–997.10.1080/00206814.2017.1363676

Casetta, F., Ickert, R.B., Mark, D.F., Bonadiman, C., Giacomoni, P. P., Ntaflos, T., and Coltorti, M., 2019, The alkaline lamprophyres of the dolomitic area (Southern Alps, Italy): Markers of the late triassic change from orogenic like to anorogenic magmatism: Journal of Petrology, v. 60, no. 6, p. 1263–-1298.10.1093/petrology/egz031

Casetta, F., Ickert, R.B., Mark, D.F., Giacomoni, P.P., Bonadiman, C., Ntaflos, T., Zanetti, A., and Coltorti, M., 2021, The Variscan subduction inheritance in the Southern Alps sub-continental lithospheric mantle: clues from the middle triassic shoshonitic magmatism of the dolomites (NE Italy): Lithos, v. 380, p. 105856. 10.1016/j.lithos.2020.105856

Cassinis, G., Cortesogno, L., Gaggero, L., Perotti, C.R., and Buzzi, L., 2008, Permian to triassic geodynamic and magmatic evolution of the brescian prealps (eastern Lombardy, Italy): Geological Society of America, v. 127, no. 3, p. 501–518

Coleman, L.C., 1978, Solidus and subsolidus compositional relationships of some coexisting skaergaard pyroxenes: Contributions to Mineralogy and Petrology, v. 66, no. 3, p. 221–227. 10.1007/BF00373406

Cottrell, E., and Kelley, K.A., 2011, The oxidation state of Fe in MORB glasses and the oxygen fugacity of the upper mantle: Earth and Planetary Science Letters, v. 305, no. 3–4, p. 270–282.10.1016/j.epsl.2011.03.014

Csontos, L., and Vörös, A., 2004, Mesozoic plate tectonic reconstruction of the Carpathian region: Palaeogeography, Palaeoclimatology, Palaeoecology, v. 210, p. 1–56.

De Min, A., Jourdan, F., Marzoli , A., Renne, P., and Juracic, M., 2009 ,The tholeiitic magmatism of Jabuka, Vis and Brusnik islands: a Carnian magmatism in the Adria Plate Rendiconti della Società Geologica Italiana, v. 9, p. 85–87.

De Min, A., Velicogna, M., Ziberna, L., Chiaradia, M., Alberti, A., and Marzoli, A., 2020, Triassic magmatism in the European Southern alps as an early phase of pangea break-up: Geological Magazine, v. 157, no. 11, p. 1800–1822. 10.1017/S0016756820000084

De Paolo, D.J., and Wasserburg, G.J., 1979, Petrogenetic mixing models and Nd-Sr isotopic patterns: Geochimica Et Cosmochimica Acta, v. 43, no. 4, p. 615–627. 10.1016/0016-7037(79)90169-8

Dobnikar, M., Dolenec, T., and Bellieni, G., 2002, Rapakivi texture in porphyritic dikes within the Karavanke granitic massif (Slovenia): Bullettin-Geological Society of Finland, v. 74, no. 1–2, p. 147–157. 10.17741/bgsf/74.1-2.007

Doglioni, C., and Carminati, E., 2008, Structural styles and Dolomites field trip: Memorie Descrittive della Carta Geologica Italiana, Vol. 82 Ist. Poligrafico dello Stato, (Torino: Geda), 299

Frost, B.R., 1991, Introduction to oxygen fugacity and its petrologic importance. Oxide minerals: petrologic and Magnetic Significance: Mineralogical Society of America "Reviews in Mineralogy", Vol. 25 (Washington: D. H. Lindsley), 1–10

Garašić, V., Vrkljan, M., Tadej, N., and Majer, V., 2001, Dolerites from the islet of Brusnik (Adriatic Sea, Croatia): Berichte der Deutschen Mineralogischen Gesellschaft, Beihefte zum European Journal of Mineralogy, v. 13, no. 1, p. 56

Giovanardi, T., Mazzucchelli, M., Zanetti, A., Langone, A., Tiepolo, M., and Cipriani, A., 2014, Occurrence of phlogopite in the Finero Mafic layered complex, Open Geosciences, v. 6, no.4, 588–613. 10.2478/s13533-012-0186-8

Golonka, J., 2004, Plate tectonic evolution of the southern margin of Eurasia in the mesozoic and cenozoic: Tectonopysics, v. 381, no. 1–4, p. 235–273.10.1016/j.tecto.2002.06.004

Golub, L., and Vragovič, M., 1975, Eruptivne stijene dalmatinskih otoka (Vis, Jabuka i Brusnik) igneous rocks of the dalmatian Islands (Vis, Jabuka and Brusnik): Acta Geologica, v. 8, no. 4, p. 19–63

Grandić, S., Kratković, I., and Balić, D., 2013, Peri-Adriatic platforms proximal Talus reservoir potential (part 1): Nafta, v. 64, no. 2, p. 147–160

Grandić, S., Kratković, I., Kolbah, S., and Samarzija, J., 2004, Hydrocarbon potential of stratigraphic and structural traps of the Ravni Kotari area - Croatia: Nafta, v. 55, no. 7–8, p. 311–327

Hart, S., and Zindler, A., 1989, Constraints on the nature and development of chemical heterogeneities in the mantle, Convection, M.ed.WR Peltier, Gordon and Breach Science Publishers: New York, 216–387

Hawthorne, F.C., Oberti, R., Harlow, G.E., Maresch, W.V., Martin, R.F., Schumacher, J.C., and Welch, M.D., 2012, Nomenclature of the amphibole supergroup, American Mineralogist, v.97, no.11–12, 2031–2048. 10.2138/am.2012.4276

Jiang, Q., Jourdan, F., Olierook, H.K., Merle, R.E., Verati, C., and Mayers, C., 2021, $^{40}Ar/^{39}Ar$ dating of basaltic rocks and the pitfalls of plagioclase alteration: Geochimica Et Cosmochimica Acta, v. 314, p. 334–357. 10.1016/j.gca.2021.08.016

Juračić, M., Novosel, A., Tibljaš, D., and Balen, D., 2004, Jabuka Shoal, a new location with igneous rocks in the Adriatic Sea: Geologia Croatica, v. 57, no. 1, p. 81–85. 10.4154/GC.2004.06

Koch, G., and Belak, M., 2003, Evaporitic-carbonate deposits of Komiža diapiric structure (Island of Vis, Croatia): Their palinostratigraphic and sedimentological features: Abstracts Book, 22nd IAS Meeting of Sedimentology Vlahović, I., 17–19SeptemberOpatija, Institute of Geology, Zagreb Opatija,:, 96

Kulušić, A., and Borojević Šostaric, S., 2014, Dinaride evaporite mélange: Diagenesis of the Kosovo polje evaporates: Geologica Croatica, v. 67, no. 1, p. 59–74. 10.4154/GC.2014.05

Le Bas, M.J., Le Maitre, R.W., and Woolley, A.R., 1992, The construction of the Total Alkali-Silica chemical classification of volcanic rocks: Mineralogy and Petrology, v. 46, no. 1, p. 1–22.10.1007/BF01160698

Li, C., Li, X., Li, Q., Guo, J., Li, X., and Liu, T., 2011, An evaluation of a single-step extraction chromatography separation method for Sm–Nd isotope analysis of micro-samples of silicate rocks by high-sensitivity thermal ionization mass spectrometry, Analytica Chimica Acta, v. 706, no. 2, 297–304. 10.1016/j.aca.2011.08.036

Li, C., Li, X., Li, Q., Guo, J., Li, X., and Yang, Y., 2012, Rapid and precise determination of Sr and Nd isotopic ratios in geological samples from the same filament loading by thermal ionization mass spectrometry employing a single-step separation scheme, Analytica Chimica Acta, v. 727, no. 54–60. 10.1016/j.aca.2012.03.040

Lu, M., Hofmann, A.W., Mazzucchelli, M., and Rivalenti, G., 1997, The mafic–ultramafic complex near Finero (Ivrea–Verbano Zone), II. Geochronology and isotope geochemistry: Chemical Geology, v. 140, no. 3–4, p. 223–235.10.1016/S0009-2541(97)00050-8

Lustrino, M., Abbas, H., Agostini, S., Caggiati, M., Carminati, E., and Gianolla, P., 2019, Origin of Triassic magmatism of the Southern Alps (Italy): Constraints from geochemistry and Sr-Nd-Pb isotopic ratios: Gondwana Research, v. 75, p. 218–238. 10.1016/j.gr.2019.04.011

Maffione, M., and van Hinsbergen, D.J.J., 2018, Reconstructing plate boundaries in the Jurassic Neo-Tethys from the East and West Vardar Ophiolites (Greece and Serbia): Tectonics, v. 37, no. 3, p. 858–887.10.1002/2017TC004790

Mancinelli, P., Scisciani, V., Pauselli, C., Stampfli, G.M., Speranza, F., and Vasiljević, I., 2022, Back-arc underplating provided crustal accretion affecting topography and sedimentation in the Adria microplate: Marine and Petroleum Geology, v. 136, p. 105470. 10.1016/j.marpetgeo.2021.105470

McCulloch, M.T., and De Dekker, P., 1989, Sr isotope constraints on the Mediterranean environment at the end of the Messinian salinity crisis: Nature, v. 342, no. 6245, p. 62–65.10.1038/342062a0

McDonough, W.F., and Sun, S.S., 1995, The composition of the Earth: Chemical Geology, v. 120, no. 3–4, p. 223–253. 10.1016/0009-2541(94)00140-4

McKenzie, D., and O'Nions, R.K., 1991, Partial Melt Distributions from Inversion of Rare Earth Element Concentrations: Journal of Petrology, v. 32, no. 5, p. 1021–1091. 10.1093/petrology/32.5.1021

Miller, C., Thöni, M., Goessler, W., and Tessadri, R., 2011, Origin and age of the Eisenkappel gabbro to granite suite (Carinthia, (SE Austrian Alps): Lithos, v. 125, no. 1–2, p. 434–448.10.1016/j.lithos.2011.03.003

Min, K., Mundil, R., Renne, P.R., and Ludwig, K.R., 2000, A test for systematic errors in $^{40}Ar/^{39}Ar$ geochronology through comparison with U/Pb analysis of a 1.1-Ga rhyolite: Geochimica Et Cosmochimica Acta, v. 64, no. 1, p. 73–98. 10.1016/S0016-7037(99)00204-5

Morimoto, N., 1988, Nomenclature of pyroxenes: Mineralogy and Petrology, v. 39, no. 1, p. 55–76.10.1007/BF01226262

Muttoni, G., Gaetani, M., Kent, D.V., Sciunnach, D., Angiolini, L., Berra, F., Garzanti, E., Mattei, M., and Zanchi, A., 2009, Opening of the Neo-Tethys Ocean and the Pangea B to Pangea A transformation during the Permian: GeoArabia, v. 14, no. 4, p. 17–48.10.2113/geoarabia140417

Neave, D.A., and Putirka, K.D., 2017, A new clinopyroxene-liquid barometer and implications for magma storage pressures under Icelandic rift zones: American Mineralogist, v. 102, no. 4, p. 777–794.10.2138/am-2017-5968

Onoue, T., Yamashita, K., Fukuda, C., Soda, K., Tomimatsu, Y., Abate, B., and Rigo, M., 2018, Sr isotope variations in the Upper Triassic succession at Pizzo Mondello, Sicily: Constraints on the timing of the Cimmerian Orogeny: Palaeogeography, Palaeoclimatology, Palaeoecology, v. 499, p. 131–137. 10.1016/j.palaeo.2018.03.025

Palinkaš, L.A., Borojević Šoštarić, S., Strmić Palinkaš, S., Crnjaković, M., Neubauer, F., Molnar, F., and Bermanec, V., 2010, Volcanoes in the Adriatic Sea: Permo-Triassic magmatism on the Adriatic–Dinaridic carbonate platform: Acta Mineralogica Petrogrographica, v. 8, p. 1–15.

Pamić, J., 1984, Triassic Magmatism of the Dinarides in Yugoslavia: Tectonophysics, v. 109, no. 3–4, p. 273–307.10.1016/0040-1951(84)90145-8

Pamić, J., Tomljenovic, B., and Balen, D., 2002, Geodynamic and petrogenetic evolution of Alpine ophiolites from the central and NW Dinarides: An overview: Lithos, v. 65, no. 1–2, p. 113–142.10.1016/S0024-4937(02)00162-7

Papike, J.J., 1974, Amphiboles and pyroxenes: Characterization of other than quadrilateral components estimates of ferric iron from microprobe data: Geological Society of America Abstracts with Programs, v. 6, p. 1053–1054.

Peacock, M.A., 1931, Classification of igneous rock series: Journal of Geology, v. 39, no. 1, p. 65–67.10.1086/623788

Pearce, J.A., and Cann, J.R., 1973, Tectonic setting of basic volcanic rocks determined using trace element analyses: Earth and Planetary Science Letters, v. 19, no. 2, p. 290–300. 10.1016/0012-821X(73)90129-5

Pearce, J.A., Ernst, R.E., Peate, D.W., and Rogers, C., 2021, LIP printing: Use of immobile element proxies to characterize Large Igneous Provinces in the geologic record: Lithos, v. 392, p. 106068. 10.1016/j.lithos.2021.106068

Peccerillo, A., and Taylor, S.R., 1976, Geochemistry of Eocene calc-alkaline volcanic rocks from the Kastamonu area, northern Turkey: Contributions to Mineralogy and Petrology, v. 58, no. 1, p. 63–81. 10.1007/BF00384745

Peressini, G., Quick, J.E., Sinigoi, S., Hofmann, A.W., and Fanning, M., 2007, Duration of a Large Mafic Intrusion and Heat Transfer in the Lower Crust: A SHRIMP U–Pb Zircon Study in the Ivrea–Verbano Zone (Western Alps, Italy: Journal of Petrology, v. 48, no. 6, p. 1185–1218. 10.1093/petrology/egm014

Pikelj, K., Hernitz-Kučenjak, M., Aščić, S., and Uračić, M., 2015, Surface sediment around the Jabuka Islet and the Jabuka Shoal: Evidence of Miocene tectonics in the Central Adriatic Sea: Marine Geology, v. 359, p. 120–133. 10.1016/j.margeo.2014.11.003

Plank, T., 2014, The chemical composition of subducting sediments: The Crust, Treatise on Geochemistry, 2nd, Vol. 4 Rudnick, R. L. (Oxford: Elsevier), 607–629

Putirka, K., 2008, Thermometers and barometers for volcanic systems: Reviews in Mineralogy and Geochemistry, v. 69, no. 1, p. 1–8. 10.2138/rmg.2008.69.1

Putirka, K., 2016, Amphibole thermometers and barometers for igneous systems and some implications for eruption mechanisms of felsic magmas at arc volcanoes: American Mineralogist, v. 101, no. 4, p. 819–840. 10.2138/am-2016-5402

Renne, P.R., Balco, G., Ludwig, K.R., Mundil, R., and Min, K., 2011, Geochimica et Cosmochimica Acta, v. 75, no. 17, p. 5097–5100. 10.1016/j.gca.2011.06.021

Renne, P.R., Mundil, R., Balco, G., Min, K., and Ludwig, K.R., 2010, Joint determination of ^{40}K decay constants and $^{40}Ar^*/^{40}K$ for the Fish Canyon sanidine standard, and improved accuracy for $^{40}Ar/^{39}Ar$ geochronology: Geochimica Et Cosmochimica Acta, v. 74, no. 18, p. 5349–5367. 10.1016/j.gca.2010.06.017

Rudnick, and R.L., Gao, S. , 2003, Composition of the continental crust: The Crust, ed. RL Rudnick, 3 Holland, H.D., Turekian, K.K. Treatise in Geochemistry (Oxford: Oxford University Press), Vol:3, 1–64.

Sassi, R., Mazzoli, C., Merle, R., Brombin, V., Chiaradia, M., Dunkley, D.J., and Marzoli, A., 2020, HT–LP crustal syntectonic anatexis as a source of the Permian magmatism in the Eastern Southern Alps: Evidence from xenoliths in the Euganean trachytes (NE Italy): Journal of the Geological Society, v. 177, no. 6, p. 1211–1230. 10.1144/jgs2020-031

Schettino, A., and Turco, E., 2011, Tectonic history of the western Tethys since the Late Triassic: Geological Society of America Bulletin, v. 123, no. 1–2, p. 89–105.10.1130/B30064.1

Schmid, S.M., Bernoulli, D., Fügenschuh, B., Matenco, L., Schefer, S., Schuster, R., Tischler, M., and Ustaszewski, K., 2008, The Alpine-Carpathian-Dinaric orogenic system: Correlation and evolution of tectonic units: Swiss Journal of Geoscience, v. 101, no. 1, p. 139–183.10.1007/s00015-008-1247-3

Shaw, H.F., and Wasserburg, G.J., 1985, Sm-Nd in marine carbonates and phosphates: Implications for Nd isotopes in seawater and crustal ages: Geochimica et Cosmochimica Acta, v. 49, no. 2, p. 503–518.10.1016/0016-7037(85)90042-0

Slovenec, D., Lugovic, B., Meyer, H.P., and Garapic, G., 2011, A tectono-magmatic correlation of basaltic rocks from ophiolite melanges at the north-eastern tip of the Sava-Vardar Suture Zone, northern Croatia, constrained by geochemistry and petrology: Ofioliti, v. 36, no. 1, p. 77–100

Slovenec, D., and Šegvić, B., 2018, The first ultramafic cumulates from Mt. Kalnik ophiolite mélange in the SW part of the Zagorje-Mid-Transdanubian Zone (NW Croatia): Mineralogy, petrology, geochemistry and tectono-affinity : Geologia Croatica, v. 71, no. 3, p. 185–197. 10.4154/GC.2018.17

Slovenec, D., and Šegvić, B., 2021, Middle Triassic high-K calc-alkaline effusive and pyroclastic rocks from the Zagorje-Mid-Transdanubian Zone (Mt. Kuna Gora; NW Croatia): Mineralogy, petrology, geochemistry and tectonomagmatic affinity, Geologica Acta, Vol. 19, no. 2, 1–23. 10.1344/GeologicaActa2021.19.2

Spera, F.J., and Bohrson, W.A., 2001, Energy-constrained open-system magmatic processes I: General model and energy-constrained assimilation and fractional crystallization (EC-AFC) formulation: Journal of Petrology, v. 42, no. 5, p. 999–1018. 10.1093/petrology/42.5.999

Stampfli, G.M., and Borel, G.D., 2002, A plate tectonic model for the Paleozoic and Mesozoic constrained by dynamic plate boundaries and restored synthetic oceanic isochrons: Earth and Planetary Science Letters, v. 196, no. 1–2, p. 17–33.10.1016/S0012-821X(01)00588-X

Stampfli, G.M., and Kozur, H., 2006, Europe from the Variscan to the Alpine cycles, Gee, D.G., and Stephenson, R., eds., European lithosphere dynamics, Geological Society: London, Memoir, Vol. 32, 57–82 p.

Storck, J.C., Brack, P., Worzlaw, J.F., and Ulmer, P., 2019, Timing and evolution of Middle Triassic magmatism in the Southern Alps (northern Italy): Journal of the Geological Society, v. 176, no. 2, p. 253–268.10.1144/jgs2018-123

Sun, S.S., and McDonough, W.F., 1989, Chemical and isotopic systematics of oceanic basalts: Implications for mantle composition and processes: Magmatism in the Ocean Basins, Geological Society of London Special Publication, London: Vol. 42 Saunders, A. D., Norry, M.J., 313–345.

Verati, C, and Jourdan, F., 2014, Modelling effect of sericitization of plagioclase on the $^{40}K/^{40}Ar$ and $^{40}Ar/^{39}Ar$ chronometers: implication for dating basaltic rocks and mineral deposits. Geological Society, London, Special Publications, 378, no.1, 155–174. 10.1144/SP378.14

Visonà, D., and Zanferrari, A., 2000, Some constraints on geochemical features in the Triassic mantle of the easternmost Austroalpine-Southalpine domain: Evidence from the Karawanken pluton (Carinthia, Austria): International Journal of Earth Science, v. 89, no. 1, p. 40–51.10.1007/s005310050316

Vlahović, I., Tišljar, J., Velić, I., and Matičec, D., 2005, Evolution of the Adriatic Carbonate Platform: Palaeogeography, main events and depositional dynamics: Palaeogeography, Palaeoclimatology, Palaeoecology, v. 220, no. 3–4, p. 333–360. 10.1016/j.palaeo.2005.01.011

Wood, D.A., 1980, The application of a Th-Hf-Ta diagram to problems of tectonomagmatic classification and establishing the nature of crustal contamination of basaltic lavas of the British Tertiary volcanic province: Earth and Planetary Science Letters, v. 50, no. 1, p. 11–30.10.1016/0012-821X(80)90116-8

Workman, R.K., and Hart, S.R., 2005, Major and trace element composition of the depleted MORB mantle (DMM): Earth and Planetary Science Letters, v. 231, no. 1–2, p. 53–72.10.1016/j.epsl.2004.12.005

Yokoyama, T., Makishima, A, and Nakamura, E., 1999, Evaluation of the coprecipitation of incompatible trace elements with fluoride during silicate rock dissolution by acid digestion, Chemical Geology, 157(3–4), 175–187. 10.1016/S0009-2541(98)00206-X

Zanetti, A., Mazzucchelli, M., Rivalenti, G., and Vannucci, R., 1999, The Finero phlogopite-peridotite massif: An example of subduction-related metasomatism: Contributions to Mineralogy and Petrology, v. 134, no. 2, p. 107–122. 10.1007/s004100050472